James F. Klapproth
Manager, Engineering and Technology

Nuclear Services
General Electric Company
175 Curtner Avenue, MC 706, San Jose, CA 95125-1088
408 925-5434, Fax: 408 925-3837
james.klapproth@gene.ge.com

MFN 01-071
December 18, 2001

Document Control Desk
U.S. Nuclear Regulatory Commission
Washington, D.C. 20555

Subject: Submittal of GE Non-Proprietary Document NEDO-32983-A, **General Electric Methodology for Reactor Pressure Vessel Fast Neutron Flux Evaluations,** December 2001.

Reference: MFN 00-070, Submittal of GE Proprietary Document NEDC 32983P-A, Revision 1, **General Electric Methodology for Reactor Pressure Vessel Fast Neutron Flux Evaluations,** December 14, 2001.

GE submitted the reference document , NEDC 32983P-A, Revision 1, to the NRC on December 14, 2001. The enclosed document (1 copy), NEDO 32983-A, is the non-proprietary version of the reference.

Sincerely,

J. F. Klapproth, Manager
Engineering and Technology
GE Nuclear Energy
(408) 925-5434
e-mail: james.klapproth@gene.ge.com

cc: J. Donoghue (NRC) w Attachments (1copy + 1 CD)
S. Sitaraman (GE) w/o Attachments

Attachment: NEDO-32983-A

T007

GE Nuclear Energy

NEDO-32983-A
Revision 0
DRF A41-00107-00
Class I
December 2001

Licensing Topical Report

General Electric Methodology for Reactor Pressure Vessel Fast Neutron Flux Evaluations

S. Sitaraman
S. Wang
T. Wu

GE Nuclear Energy

175 Curtner Avenue
San Jose, CA 95125

NEDO-32983-A
Revision 0
DRF A41-00107-00
Class I
December 2001

LICENSING TOPICAL REPORT

GENERAL ELECTRIC METHODOLOGY FOR REACTOR PRESSURE VESSEL FAST NEUTRON FLUX EVALUATIONS

Prepared by:

S. Sitaraman
S. Wang
T. Wu

Approved: 

J. F. Klapproth, Manager
Engineering & Technology

IMPORTANT NOTICE REGARDING CONTENTS OF THIS REPORT

PLEASE READ CAREFULLY

The information contained in this document is furnished for the purpose of obtaining NRC approval of a calculation process for determining the reactor pressure vessel neutron fluence. The only undertakings of General Electric Company respecting information in this document are contained in the contracts between General Electric Company and the participating utilities in effect at the time this report is issued, and nothing contained in this document shall be construed as changing those contracts. The use of this information by anyone other than that for which it is intended is not authorized; and with respect to **any unauthorized use**, General Electric Company makes no representation or warranty, and assumes no liability as to the completeness, accuracy, or usefulness of the information contained in this document.

UNITED STATES
NUCLEAR REGULATORY COMMISSION
WASHINGTON, D.C. 20555-0001

September 14, 2001

Mr. James F. Klapproth, Manager
Engineering & Technology
GE Nuclear Energy
175 Curtner Ave
San Jose, CA 95125

MFN 01-050

SUBJECT: SAFETY EVALUATION FOR NEDC-32983P, "GENERAL ELECTRIC METHODOLOGY FOR REACTOR PRESSURE VESSEL FAST NEUTRON FLUX EVALUATION" (TAC NO. MA9891)

Dear Mr. Klapproth:

By letter dated September 1, 2000, GE Nuclear Energy (GENE) submitted the subject licensing topical report (LTR) and requested staff review and approval for boiling water reactor (BWR) licensing actions. Additional information was submitted on December 20, 2000, January 5 and 17, 2001, March 2 and 14, 2001, and June 1 and 15, 2001. The NRC staff and Brookhaven National Laboratory (BNL staff consultant) exchanged information with GENE personnel on several occasions in the course of this review.

The proposed methodology employs an analytic approach based on the discrete ordinates neutron transport method to determine the fast (E > 1.0 MeV) flux (and fluence) in BWR vessels. The proposed methodology adheres to the guidance in Regulatory Guide (RG) 1.190, "Calculational and Dosimetry Methods for Determining Pressure Vessel Neutron Fluence." The method is using available BWR surveillance capsule dosimetry measurements for the validation of the analytic transport calculations and the estimation of the uncertainty and bias. In addition, the method is compared to the NUREG-6115 benchmark problem and the results of a foreign reactor benchmark provided by GENE.

The staff finds the proposed methodology acceptable for referencing in licensing actions, subject to the limitation that the applicant will demonstrate the method's predictive capability in at least four surveillance capsules within three years from the day of approval of this methodology. The LTR includes a limited amount of information on the method's capability to predict the fluence on and through the core shroud. The staff concluded that the method would yield a conservative fluence estimate on the shroud. In view of the shroud fluence requirements, the staff finds the method acceptable subject to the limitations listed in the summary and limitations section of the enclosed safety evaluation (SE).

A conference call was held on August 14, 2001 between GENE, BNL and the NRC staff to discuss GENE's findings from their review of the draft SE (ADAMS accession no. ML012410011) regarding proprietary information. The conference call determined that there was no proprietary information contained in the SE. GENE requested clarification on the three year requirement for the confirmatory and predictive dosimetry for the vessel and the shroud. The staff stated that: (1) the measurement to calculation comparisons need only include activation dosimetry, (2) RG 1.190 contains the required guidance, and (3) GENE must prepare and submit to the staff a plan, identifying proposed surveillance capsules and a time schedule to satisfy and erase the limitations from the methodology.

The NRC requests that the GENE publish an accepted version of the revised NEDC-32983P within 3 months of receipt of this letter. The accepted version shall incorporate this letter and the enclosed SE between the title page and the abstract, and add an "-A" (designating accepted) following the report identification number (i.e., NEDC-32983-A).

If the NRC's criteria or regulations change so that its conclusion in this letter that the LTR is acceptable is invalidated, GENE and/or the applicant referencing the LTR will be expected to revise and resubmit its respective documentation, or submit justification for the continued applicability of the LTR without revision of the respective documentation.

If you have any questions, please contact Robert Pulsifer, GENE Project Manager, at (301) 415-3016.

Sincerely,

FOR

Stuart A. Richards, Director
Project Directorate IV
Division of Licensing Project Management
Office of Nuclear Reactor Regulation

Project No. 710

Enclosure: Safety Evaluation

cc w/encl: See next page

cc:
Mr. George B. Stramback
Regulatory Services Project Manager
GE Nuclear Energy
175 Curtner Avenue
San Jose, CA 95125

Mr. Charles M. Vaughan, Manager
Facility Licensing
Global Nuclear Fuel
P.O. Box 780
Wilmington, NC 28402

Mr. Glen A. Watford, Manager
Nuclear Fuel Engineering
Global Nuclear Fuel
P.O. Box 780
Wilmington, NC 28402

UNITED STATES
NUCLEAR REGULATORY COMMISSION
WASHINGTON, D.C. 20555-0001

SAFETY EVALUATION BY THE OFFICE OF NUCLEAR REACTOR REGULATION

GE NUCLEAR ENERGY TOPICAL REPORT NEDC-32983P

"GENERAL ELECTRIC METHODOLOGY FOR REACTOR PRESSURE VESSEL FAST NEUTRON FLUX EVALUATIONS"

PROJECT NO. 710

1.0 INTRODUCTION

By letter dated September 1, 2000, GE Nuclear Energy (GENE) submitted their methodology for reactor pressure vessel fast neutron flux evaluations and requested NRC review and approval (Reference 1). The proposed methodology is intended for the determination of the fast neutron fluence accumulated by the pressure vessel and internal components of US boiling water reactor (BWR) plants. The methodology has evolved from earlier GENE fluence methods. The proposed licensing topical report (LTR) (NEDC-32983P) fluence evaluation employs an analytic approach using the most recent fluence calculational methods and nuclear data sets. In the proposed methodology, the vessel fluence is determined by a discrete ordinates transport calculation in which the core neutron source is explicitly represented and the neutron flux is propagated from the core through the downcomer and the jet pumps and jet pump risers whenever present, to the vessel (rather than by an extrapolation of the measurements). The method proposed for predicting the dosimeter response and the vessel inner-wall fluence is generally consistent with Regulatory Guide (RG) 1.190, "Calculational and Dosimetry Methods for Determining Pressure Vessel Neutron Fluence" (Reference 2).

The LTR provides a description of the application of the proposed methodology to the calculation of the Brookhaven National Laboratory (BNL) pressure vessel fluence benchmark problem described in NUREG/CR-6115 (Reference 3). The LTR also describes the application of the methodology to the analysis of a GENE dosimetry benchmark experiment (References 4 and 5). This includes a description of both the discrete ordinates DORT (Reference 6) and the MCNP (Reference 7) Monte Carlo transport calculations of the measurements and the techniques used to interpret the in-vessel dosimeter response. Representative BWR surveillance measurements and comparisons to GENE calculations are provided as additional qualification of the calculational methods. The GENE dosimetry measurements are used to validate the DORT vessel fluence methodology and determine the calculational biases and uncertainties.

The LTR fluence calculation and uncertainty methodology is summarized in Section 2. The evaluation of the important technical issues raised during this review is presented in Section 3 and the summary and limitations given in Section 4. The staff was assisted in this review by BNL personnel as consultants.

2.0 SUMMARY OF THE NEDC-32983P VESSEL FLUENCE METHODOLOGY

2.1 Pressure Vessel Fluence Calculation Methodology

The proposed methodology provides a best-estimate prediction of the fluence rather than the conservative prediction as was the case with earlier methods. The fluence calculations are performed with the DORT discrete ordinates transport code. The LTR provides a description of the DORT calculation used to determine the vessel fluence, as well as the calculations used to predict the GENE measured dosimetry and validate the transport model. The calculational model includes a representation of the peripheral fuel assemblies and the core-internals, downcomer and vessel geometry. Calculations are performed to determine the pin-by-pin and bundle-average power distribution in the peripheral fuel bundles for input to the DORT core neutron source. Calculations employ a relatively fine (r, θ, z) spatial mesh and are carried out using both an S_8 and an S_{12} angular quadrature set.

The eighty-group MATXS (Reference 8) cross section library is the basic nuclear data set. This library is used in performing the energy and spatial self-shielding and removal calculations. The scattering cross sections are represented using a P_3 Legendre expansion. The calculations are performed in (r, θ) and (r, z) geometries. A synthesis technique is used to determine the three-dimensional fluence distribution and to some extent account for the effect of axial leakage between the core and the cavity.

Predictions of the dosimeter response measurements are required to determine the calculation-to-measurement (C/M) data base used to validate the fluence calculation methods. The predictions are made for the in-vessel dosimetry using essentially the same methods used to determine the vessel fluence. The proposed methodology includes dosimeter response adjustments for the half-lives of the reaction products and the core power history. In order to ensure an accurate prediction of the dosimeter response, a detailed spatial representation of the capsule geometry is included in the DORT model. The measured dosimeter reaction rates are calculated using the dosimeter-specific reaction cross sections. The calculated dosimeter response is determined for the irradiation period up to the time the capsule was withdrawn.

2.2 Calculation of the BNL Pressure Vessel Fluence Benchmark Problem

As part of the qualification of the fluence calculational methodology, GENE has calculated the BNL NUREG/CR-6115 BWR pressure vessel fluence benchmark problem. The NUREG/CR-6115 report provides the detailed specification and corresponding numerical solutions for the BWR fluence benchmark problem. The calculation of the benchmark problem allows a detailed assessment and verification of the numerical procedures, code implementation, and the various modeling approximations relative to a representative BWR operating configuration. The geometry, materials and space and energy dependent source are fixed by the problem specification and the reference solutions allow comparisons of the predicted fluence at the vessel locations of interest.

The LTR describes the calculations performed using both the proposed DORT discrete ordinates method and the MCNP Monte Carlo method. The DORT calculations were performed using the proposed "current" method. The calculational model included the complete radial geometry from the core out through the concrete biological shield and axially from the core inlet

up to the steam separator. As part of the analysis of the benchmark problem, GENE performed a series of sensitivity calculations in which various modeling assumptions were evaluated. Calculations were performed with three downcomer models: (1) a conservative model in which the jet pumps and risers are neglected, (2) an approximate model in which the materials of the jet pumps and risers are homogenized over the volume of the downcomer, and (3) a model in which the components in the downcomer are treated explicitly as heterogeneous material zones. Calculations were performed using both ENDF/B-V and ENDF/B-VI nuclear data sets. The effect of using a more accurate angular quadrature set was evaluated by comparing calculations performed with S_8 and S_{12} quadratures. The effect of the peripheral radial flux gradient on the core neutron source and vessel fluence was evaluated by calculating the fluence with: (1) a model in which a uniform bundle-average power is assigned to each peripheral fuel bundle, and (2) a model in which spatially dependent power distributions (provided with the problem specification) are assigned to the outer three rows of fuel bundles.

Comparisons of the GENE and BNL NUREG/CR-6115 vessel fluence predictions are provided. As an additional verification of the GENE fluence methodology, GENE has performed MCNP Monte Carlo calculations of the BNL vessel fluence benchmark problem. The MCNP model included an essentially exact octant representation of the core, shroud, jet pump/riser and vessel geometry specified in the NUREG/CR-6115 report. The calculations were performed using a continuous energy representation of the nuclear data. The cross section data used in these calculations is based on the ENDF/B-V nuclear data except for iron, hydrogen and oxygen. Since the cross sections for these elements have changed significantly in the more recent ENDF/B-VI data set, ENDF/B-VI cross sections were used for iron, hydrogen and oxygen. Calculations were performed using two models for describing the power/source distribution in the peripheral fuel bundles: (1) a uniform bundle-average power model, and (2) a pin-wise power distribution model. The source normalization used in the MCNP calculation was taken to be the same as that used in the DORT calculation of the benchmark problem. Variance reduction was accomplished by defining a set of importance regions which allowed particle splitting. In addition to the base calculation, a series of MCNP sensitivity calculations was performed to determine the effect of: (1) including the jet pumps and riser materials, (2) variations in the fuel actinide inventory, and (3) the ENDF/B-V to ENDF/B-VI cross section updates.

The LTR includes comparisons of the GENE and BNL NUREG/CR-6115 MCNP fluence predictions. Comparisons are provided for the $E > 1.0$ MeV fluence at the axial midplane for locations in the downcomer and on the vessel inner-wall.

2.3 Calculation of the BWR Neutron Dosimetry Benchmark Measurements

In order to provide a measurement benchmark for qualifying the DORT and MCNP calculational methodology, GENE has performed an in-reactor dosimetry benchmark experiment (References 4 and 5). The experiment included the irradiation of a set of passive dosimeters for one cycle in an operating (non-US) BWR. The measurements included Fe-54, Nb-93, and Ni-58 threshold dosimeters as well as U-238, Th-232 and Np-237 fission dosimeters. The dosimeters were located in the downcomer at three axial elevations, three azimuths and three radial locations. The dosimeter activation counting and related measurements were performed at the GE Vallecitos Nuclear Laboratory.

The neutron dosimetry provides a direct measurement of the activity (dps/gm) associated with the individual dosimeter-specific reactions. The measured dosimeter activities were converted to specific full power reaction rates (rps/nucleus) averaged over the period of irradiation. This conversion accounted for the physical characteristics of the sensor (e.g., weight of the target isotope in the sample), the operating history of the reactor, the energy response of the sensor (e.g., reaction cross section), decay of the target isotope, and in the case of fission dosimeters, the number of product atoms produced per reaction. In order to allow comparison of the measured and calculated dosimeter reaction rates, the measured reaction rates have also been corrected for target depletion.

The in-vessel dosimetry measurements were used to benchmark and validate the proposed calculational methodology. The validation included both DORT and MCNP calculations of the measured dosimeter reaction rates. The calculational models used in the prediction of the measurements are based on the proposed methodology described in Section 2.1. The models include a detailed representation of the peripheral fuel assemblies and the core internals, downcomer and vessel geometry. The DORT calculations employ a relatively fine (r, θ, z) spatial mesh and were carried out using an S_{12} quadrature and a P_3 expansion of the scattering cross sections.

The calculations of the dosimeter response measurements are used to determine the calculation-to-measurement data base used to validate the fluence calculation methods. The analysis of the C/M data indicates that: (1) the DORT calculations using an adjusted downcomer model result in a mean C/M value ranging from 0.9 to 1.1 for Fe-54 and Nb-93, and (2) the MCNP calculations result in C/M values ranging from 0.9 to 1.1.

3.0 EVALUATION

The review of the NEDC-32983P methodology focused on the details of the fluence calculation methods, their compliance with the guidance in RG 1.190 and the qualification of the methodology provided by the GENE C/M data-base. As a result of the review, several technical issues were identified which required additional information and clarification from GENE. Requests for additional information (RAI) were transmitted in References 9, 13 and 16. The GENE responses were provided in References 10-12, 14-15, and 17-18. This evaluation is based on the material included in the LTR and in the referenced GENE responses to the RAIs. The evaluation of the major issues raised during the review is summarized in the following.

3.1 Pressure Vessel Fluence Calculation Methodology

The DORT transport calculational model is constructed using plant-specific as-built dimensions and actual plant parameters whenever possible (response to RAI-5, Reference 10). The calculations use a fine spatial and angular mesh in both the (r, θ) and (r, z) calculations together with a detailed representation of the core internals, downcomer, and vessel geometry. The calculations employ an S_8 angular quadrature set and a P_3 scattering cross section expansion.

The proposed fluence methodology generally employs a best-estimate approach, however, certain conservative features have been retained from the traditional method. For example, in response to RAI-2 (Reference 10), GENE indicates that the core neutron source used in the

DORT transport calculation is based on the bundle-average power in the peripheral fuel bundles. This results in a conservatism in the fluence estimate because: (1) the fuel pins close to the core edge have reduced power because of neutron leakage from the core, and (2) the fuel pins close to the core edge provide the dominant contribution to the vessel fluence. The magnitude of the effect of using the bundle-average power rather than the pin-wise power distribution is calculated for the BWR pressure vessel fluence benchmark problem (Reference 3). In addition, in the response to RAI-2 (Reference 15), GENE indicated that this conservatism in the fluence calculation is applicable to all core designs. However, GENE has indicated in response to RAI-18 (Reference 10) that credit for this conservatism will be taken in determining the adjustment that must be applied to the calculated fluence to determine the best-estimate fluence value. Therefore, while the proposed current methodology includes this conservatism and over-predicts the fluence due to the use of bundle-average power, this conservatism is removed in the application of the methodology when the best-estimate fluence is determined, by a downward adjustment of the calculated fluence.

The nuclear cross section library used in the fluence transport calculations employs a P_3 Legendre expansion of the anisotropic cross sections. However, because of the relatively strong axial dependence of the void distribution in the core and the presence of the jet-pump and jet-pump riser arrangement in the downcomer, there was concern that the third order Legendre expansion may not be sufficiently detailed to accurately model the streaming and shadowing effects at the vessel inner-wall. In order to evaluate this effect, GENE has performed a series of sensitivity calculations using a P_5 expansion of the anisotropic scattering cross section. The results of these calculations are presented in the response to RAI-7 (Reference 10) and indicate that the effect of this approximation on the vessel fluence and dosimetry reaction rates is negligible.

3.2 Calculation of the BNL Pressure Vessel Fluence Benchmark Problem

The BNL pressure vessel fluence benchmark problem was calculated as part of the validation and testing of the NEDC-32983P fluence methodology. The calculations were carried out using the proposed GENE methodology (response to RAI-5, Reference 2) and were compared with the tabulated benchmark reference predictions. The analysis of the benchmark problem included a set of sensitivity calculations which evaluated and confirmed the validity of several modeling assumptions included in the methodology. The GENE and reference calculations of the vessel peak inner-wall fluence were found to be in good agreement.

In the proposed methodology, the DORT transport calculations are performed using a nuclear cross section set that has been collapsed by averaging the nuclear data over a multi-group energy structure. Following the guidance in RG 1.190 (Section-1.1.2.2), GENE tested and evaluated the averaging procedure used in collapsing the cross sections. The evaluation included a series of DORT transport calculations which were carried out for the BNL vessel fluence benchmark problem using several sets of collapsed cross sections. The results of these calculations are included in the GENE response to RAI-3 (Reference 10). Calculations were performed for a 26-group cross section set, a 44-group cross section set and a 47-group cross section set (calculated by BNL). Comparisons of the $E > 1.0$ MeV flux and the flux spectrum were made at the shroud, downcomer, surveillance capsule, vessel inner-wall, vessel quarter-thickness and vessel outer-wall locations. Based on these comparisons and additional calculations performed by GENE, it is concluded that the use of the collapsed cross section

library introduces a bias into the fluence prediction (response to RAI-3, Reference 10). GENE has indicated in response to RAI-18 (Reference 10) that, in order to account for this approximation, the fluence calculated with the NEDC-32983P methodology will be adjusted to determine the best-estimate fluence value. Therefore, while the proposed current methodology includes this calculational bias due to the cross section averaging procedure, this bias will be removed when the best-estimate fluence is determined.

3.3 Calculation of the BWR Benchmark Dosimetry Measurements

The BWR neutron dosimetry experiment includes an extensive set of in-vessel fast and thermal neutron dosimeter measurements. The irradiation of the dosimeters was performed during a single cycle of operation at an operating BWR. The dosimeter activation and associated measurements were performed at the GE Vallecitos Nuclear Laboratory. The inferred reaction rates are proportional to the measured specific activities and include adjustments for the actual plant operating history and the decay of the reaction product isotope. The reaction rates were used to construct the C/M benchmark data base and determine the calculational bias and uncertainty.

The initial analysis of the BWR neutron dosimetry experiment did not include C/M comparisons for the dosimetry measurements at the 71° azimuth. However, in response to RAI-9 (Reference 15), GENE has updated the C/M data base to include this data. This additional C/M data is generally consistent with data taken at 4° and 20°. In order to allow valid benchmarking C/M comparisons of the calculations and the dosimetry experiment measurements, reliable estimates of the uncertainty in the dosimetry measurements are required. In response to RAI-11 (Reference 11), GENE has provided the uncertainty analysis for the dosimetry experiment measurements. The statistical uncertainty in the specific dosimeter activity measurement is provided for both the fast and thermal dosimeters. The measurement uncertainty resulting from the uncertainty in the capsule location is based on: (1) the mechanical tolerance for capsule displacement, and (2) the sensitivity of the dosimeter response to capsule displacement. Since the spatial variation of the fast and thermal flux (and associated displacement sensitivity) is different, the measurement uncertainty due to capsule displacement is determined for both the fast and thermal dosimeters.

In addition to the BWR neutron dosimetry experiment, the GENE dosimetry benchmark data base includes a set of surveillance capsule flux measurements. This surveillance capsule data base includes a range of plant measurements that have been made over the past decade. The activity measurements were carried out using a set of standard fast neutron threshold dosimeters. The GE Vallecitos Nuclear Laboratory analyzed the activity measurements and determined the analysis uncertainty. The activation measurement is converted to flux using a dosimeter specific cross section determined by a series of specially controlled experiments. In response to RAI-3 (Reference 14), GENE has indicated that the methods used to analyze these surveillance dosimetry measurements are compliant with the ASTM standards for measuring fast-neutron reaction rates by radioactivation of iron, copper and nickel; ASTM E-263-93 (Reference 19), ASTM E-523-92 (Reference 20) and ASTM E-264-92 (Reference 21), respectively.

3.4 C/M Comparisons and Uncertainty Analysis

The qualification of the NEDC-32983P pressure vessel neutron fluence methodology includes comparisons of fluence calculations and measurements for: (1) the operating reactor benchmark dosimetry experiment and (2) the BWR surveillance capsule dosimetry measurements. The methods benchmarking is based on both the BWR dosimetry experiment and the surveillance capsule measurements. The benchmark experiment measurements include a set of fast neutron threshold dosimeters located in the downcomer at three axial elevations, three azimuths and three radial locations. The BWR surveillance measurements are for capsules located at various locations in the downcomer including within the shadow and the penumbra of the jet pumps and jet pump risers. The dosimetry experiment provides a continuous fluence measurement during the single cycle of irradiation, while the surveillance capsule measurements provide a continuous fluence measurement from initial startup to the time of capsule removal which represent a variety of irradiation time intervals. These operating reactor measurements provide an indication of the effect of the as-built geometry and material compositions on the fluence calculations. The benchmarking is based on the calculation-to-measurement (C/M) comparisons of the measured reaction rates. The measurements provide a number of C/M comparisons and a statistical estimate of the calculational bias and uncertainty.

The benchmark experiment comparisons are made for each location as a function of dosimeter type (e.g., Fe-54 and Nb-93). In the response to RAIs 10 and 14 (Reference 12), GENE has provided the C/M ratios and analysis for the dosimetry benchmark experiment. In addition to the Fe-54 and Nb-93 bare capsule dosimeters included in the LTR, Ni-58 and Nb-93 shielded capsules were also evaluated. The C/M analysis for the dosimetry benchmark experiment indicates that the calculations are within 20 percent (one-σ) for the vessel measurements.

In the responses to RAI-17 (Reference 12) and RAI-7 (Reference 15), GENE has provided a statistical analysis of the C/M comparisons for the BWR capsule surveillance measurements. The analysis included in the responses to RAIs 17 and 18 (Reference 12) and RAI-7 (Reference 15) indicates that the proposed methodology is biased relative to the measurements. The C/M bias and its uncertainty have been determined using statistical techniques. In the proposed methodology, the best-estimate fluence is determined by applying the C/M bias to the calculated fluence. In addition, GENE has indicated in response to RAI-8 (Reference 15) that as new measurements become available these comparisons will be updated. If necessary, the bias and its uncertainty will be updated and the adjustment to the calculated fluence will be revised.

In order to provide an independent estimate of the bias and uncertainty in the NEDC-32983P fluence calculational methodology, GENE has performed an analytic uncertainty estimate. The significant sources of bias/uncertainty were identified by a set of DORT fluence sensitivity calculations. These calculations concerned the treatment of the nuclear cross section data, core neutron source, angular quadrature, and geometrical representation of the downcomer. In addition, in response to RAI-6 (Reference 15), GENE has included the effect of the BWR fuel bundle nodal and pin-wise power distribution uncertainty on the calculated fluence. Estimates of the important uncertainty contributors were made and the effect of these uncertainties was propagated through the fluence calculation using the calculated sensitivities. In the response to

RAI-18 (Reference 12) and RAI-6 (Reference 15), the analytically determined fluence calculational uncertainty is shown to be less than 20 percent.

The significant sources of calculational bias were determined to be: (1) the effect of using the bundle-average power rather than the pin-wise power distribution in the peripheral fuel bundles, and (2) the effect of using a specific flux-averaged multi-group cross section set. In the response to RAI-18 (Reference 12), the overall fluence calculational bias is determined analytically as a combination of these individual components. The bias determined using the analytic method was found to be slightly less but well within the uncertainty range of the bias determined based on the surveillance dosimetry measurements. In the conclusion of the response to RAI-7 (Reference 15), GENE stated that the calculational bias based on the dosimetry measurements will be applied to the fluence calculated using the NEDC-32983P fluence methodology.

While the uncertainty analysis based on the surveillance dosimetry C/M comparisons is generally consistent with the analytic uncertainty, it is noted that several substantial adjustments are required to account for approximations made in the calculations of the surveillance data. In addition the uncertainty in the fluence adjustment is not substantially smaller than the adjustment itself. Therefore, in order to provide additional confidence in the benchmarking of the proposed fluence methodology, within three years GENE is required to perform predictive calculations of at least four additional BWR capsule dosimetry activity measurements. These calculations should be submitted to the NRC staff prior to the completion of the measurements. After the measurements are completed, comparisons of the measurements and calculations should also be submitted to the NRC. If the C/M comparisons are not consistent with the proposed NEDC-32983P fluence methodology and supporting benchmark uncertainty analysis, the necessary revisions to the uncertainty analysis and methodology should be provided in the submittal. This requirement was discussed and agreed upon with GENE in a NRC/GENE/BNL conference call on June 25, 2001.

3.5 Core Shroud

In addition to the calculation of pressure vessel fluence, GENE has indicated that the proposed fluence methodology may be required for material evaluations of the core shroud. GENE has described the shroud fluence calculational procedure and provided an analytic estimate of the calculational uncertainty in response to RAI-8 (Reference 17).

As benchmarking for the shroud fluence calculation, in Figure 5-4 of the LTR and in the response to RAI-8 (Reference 17), GENE has provided comparisons of reaction rates calculated with the proposed methodology and reaction rates determined from measurements for capsules located close to the shroud. No direct shroud data were provided. The benchmark experiment C/M comparisons for the shroud indicate a conservative bias and a systematic over-prediction of the measurement data. However, review of this data indicates that the C/M comparisons for these dosimeters include large differences that are outside the expected calculation and measurement uncertainties. Consequently, because the bias is based on a single experiment and there is no surveillance data to confirm this result, this conservatism is not considered sufficiently reliable to reduce the calculated shroud fluence.

However, shroud fluence values are used mainly for the estimation of shroud crack growth propagation rates. The phenomenon is associated with a threshold fluence value. Therefore, the staff finds the proposed method acceptable for shroud fluence calculations provided that: (1) the estimates are limited within the beltline region, and (2) the bias is not deducted from the calculated value. To provide additional confidence to the predicted shroud fluence, GENE is required within three years from the approval of this methodology to perform and provide to the staff additional dosimetry analysis, directly related to the shroud, demonstrating the capability of this method.

4.0 SUMMARY AND LIMITATIONS

The staff reviewed NEDC-32983P entitled, "General Electric Methodology for Reactor Pressure Vessel Fast Neutron Flux Evaluations," and supporting documentation provided in References 10-12, 14-15 and 17-18. Based on this review, it is concluded that the NEDC-32983P methodology provides an acceptable best-estimate prediction of the pressure vessel neutron fluence for US BWR plants. As discussed in Section 3.4 of this SE, the best-estimate vessel fluence prediction is determined by the application of the calculated-bias adjustment to the fluence estimate using the NEDC-32983P fluence methodology.

However, this acceptance is subject to the following limitations and requirements (Sections 3.4 and 3.5):

(1) Within three years from the day of the approval of this methodology, GENE will perform predictive calculations of at least four additional BWR surveillance capsule dosimetry measurements which will be submitted to the staff before initiation of the measurements.

(2) Comparisons of the measurements and calculations will also be submitted to the NRC.

(3) Shroud fluence estimates will be limited to the beltline region, without bias adjustment.

(4) GENE will perform dosimetry analysis to confirm and remove the conservatism in the shroud fluence calculations.

(5) Revisions to the fluence methodology and supporting uncertainty analysis will be provided, if the C/M comparisons (for the additional analysis for the vessel and the shroud) are not consistent with the NEDC-32983P fluence methodology.

5.0 REFERENCES

1. "Submittal of GE Proprietary Document NEDC-32983P, General Electric Methodology for Reactor Pressure Vessel Fast Neutron Flux Evaluations," Letter, J. F. Klapproth (GENE) to USNRC, dated September 1, 2000.

2. Office of Nuclear Regulatory Research, "Calculational and Dosimetry Methods for Determining Pressure Vessel Neutron Fluence," Regulatory Guide 1.190, U.S. Nuclear Regulatory Commission, April 2001.

3. "Pressure Vessel Fluence Calculation Benchmark Problems and Solutions," NUREG/CR-6115 (BNL NUREG-52395), Brookhaven National Laboratory (to be published).

4. Terhune, J. H., Sitaraman, S., Higgins, J., P., Chiang, R-T., and Asano, K., "Neutron and Gamma Spectra in the BWR- Phase 1 Experimental and Computational Methods," Proceedings of the Fifth International Conference on Nuclear Engineering, Nice, France, ICONE5-2020, May 26-30, 1997.

5. Sitaraman, S., Chiang, R-T. , Asano, K., and Koyabu, K., "Benchmark for a 3D Monte Carlo Boiling Water Reactor Fluence Computational Package - MF3D," International Conference on Advanced Monte Carlo for Radiation Physics, Particle Transport Simulation and Applications, Lisbon, Portugal, October 23-26, 2000.

6. "DORT, Two-Dimensional Discrete Ordinates Transport Code," RSIC Computer Code Collection, CCC-484, Oak Ridge National Laboratory, 1988.

7. J. F. Breismeister (Ed.), "MCNP – A General Monte Carlo N-Particle Transport Code, Version 4A," LA-12625, Los Alamos National Laboratory, March 1994.

8. MacFarlane, R. E., Muir, D. W., "The NJOY Nuclear Data Processing System, Version 91," LA-12740-M, Los Alamos National Laboratory, October 1994.

9. "Request for Additional Information - Topical Report NEDC-32983P, General Electric Methodology for Reactor Pressure Vessel Fast Neutron Fluence Evaluations," Letter, R. M. Pulsifer (USNRC) to J. F. Klapproth (GENE), dated November 15, 2000.

10. "Completion of Responses to Request for Additional Information - GE Nuclear Energy Licensing Topical Report NEDC-32983P RAI#s: 1, 2, 3, 4, 5, 7, 8, 12, 13, 15, and 16," Letter, J. F. Klapproth (GENE) to USNRC, dated December 20, 2000.

11. "Completion of Responses to Request for Additional Information - GE Nuclear Energy Licensing Topical Report NEDC-32983P RAI# 11," Letter, J. F. Klapproth (GENE) to USNRC, dated January 5, 2001.

12. "Completion of Responses to Request for Additional Information - GE Nuclear Energy Licensing Topical Report NEDC-32983P RAI#s: 6, 9, 10, 14, 17, 18 and 19," Letter, J. F. Klapproth (GENE) to USNRC, dated January 17, 2001.

13. "Request for Additional Information - Topical Report NEDC-32983P, General Electric Methodology for Reactor Pressure Vessel Fast Neutron Fluence Evaluations," Letter, G. S. Shukla (USNRC) to J. F. Klapproth (GENE), dated February 12, 2001.

14. "Partial Response to Request for Additional Information (Round Two) - GE Nuclear Energy Licensing Topical Report NEDC-32983P," Letter, J. F. Klapproth (GENE) to USNRC, dated March 2, 2001.

15. "Completion of Responses to Request for Additional Information (Round Two) - GE Nuclear Energy Licensing Topical Report NEDC-32983P RAI#s: 1, 2, 4, 6, 7, 8, and 9," Letter, J. F. Klapproth (GENE) to USNRC, dated March 14, 2001.

16. "Request for Additional Information - Topical Report NEDC-32983P, General Electric Methodology for Reactor Pressure Vessel Fast Neutron Fluence Evaluations," Letter, R. M. Pulsifer (USNRC) to J. F. Klapproth (GENE), dated April 27, 2001.

17. "Response to Request for Additional Information - GE Nuclear Energy Licensing Topical Report NEDC-32983P RAI#'s: 1 through 8," Letter, J. F. Klapproth (GENE) to USNRC, dated June 1, 2001.

18. "Response to Request for Additional Information - GE Nuclear Energy Licensing Topical Report NEDC-32983P Verbal Request During June 8, 2001 Conference Call," Letter, J. F. Klapproth (GENE) to USNRC, dated June 15, 2001.

19. ASTM E-263-93, "Standard Test Method for Measuring Fast-Neutron Reaction Rates by Radioactivation of Iron," ASTM Standards, Section 12, American Society for Testing and Materials, Philadelphia, PA, 1995.

20. ASTM E-523-92, "Standard Test Method for Measuring Fast-Neutron Reaction Rates by Radioactivation of Copper," ASTM Standards, Section 12, American Society for Testing and Materials, Philadelphia, PA, 1995.

21. ASTM E-264-92, "Standard Test Method for Measuring Fast-Neutron Reaction Rates by Radioactivation of Nickel," ASTM Standards, Section 12, American Society for Testing and Materials, Philadelphia, PA, 1995.

Principal Contributor: Lambros Lois

Date: September 14, 2001

TABLE OF CONTENTS

TABLE OF CONTENTS
(Continued)

LIST OF TABLES

LIST OF FIGURES

LIST OF FIGURES
(Continued)

ACKNOWLEDGMENTS

The following individuals contributed significantly to the verification, development and review of this report:

B. J. Branlund

T. A. Caine

H. A. Careway

R. S. Drury

G. Gibson

M. E. Harding

J. E. Leatherman

C. L. Martin

T. R. McIntyre

J. S. Post

K. T. Schaefer

M. K. Swope

ABSTRACT

This document presents the calculation methodology developed by the General Electric Company (GE) for the determination of reactor pressure vessel fast neutron flux. The adequacy of the GE methodology is demonstrated through a detailed description of the calculation procedures and examples showing agreement between GE practices and the standards and requirements set forth in the Regulatory Guide 1.190.

Validation of the methodology is demonstrated through GE solutions to the BWR benchmark problem. Benchmark calculations of the in-reactor irradiation sample reaction rates provide additional validation. Sensitivity studies of calculation variables, as well as uncertainty and bias assessments, are also included.

A calculational bias currently exists in the GE-calculated fluences compared to data collected through surveillance samples. The improved methodology described in this LTR eliminates some of the excess conservatism and provides a more realistic flux distribution within the reactor vessel, while meeting the requirements of Regulatory Guide 1.190.

1.0 INTRODUCTION

This document presents an improved General Electric Company (GE) flux calculation methodology for determination of reactor pressure vessel (RPV) and internals neutron fluence. Similar methods and processes have been in use by GE for the past decade for the evaluation of fast neutron fluence in the reactor pressure vessel and internal components.

In order to demonstrate that the GE methodology is in agreement with the intent of Regulatory Guide 1.190 (and its draft version, DG-1053), Calculational and Dosimetry Methods for Determining Pressure Vessel Neutron Fluence [1], the following topics are covered in this report:

- GE flux synthesis methodology: Geometric and material representations of the calculation model, cross section library, neutron source distribution, etc.
- GE solution to the NUREG/CR-6115 BWR benchmark problem[2]: GE methodology comparable to Brookhaven National Laboratory (BNL) solution is used for the benchmark calculations. GE results and BNL results are compared. Sensitivity studies are performed for calculation variables including: the effects of steel components in the downcomer, ENDF[1]/B-VI vs. ENDF/B-V iron cross sections, S_8 vs. S_{12} angular quadratures, pin-by-pin vs. bundle-average power density, etc.
- Monte Carlo solution to BWR benchmark problem: Comparison of GE 3-D Monte Carlo technique vs. BNL 3-D solution.
- Benchmark through in-reactor measurements: Calculated reaction rates vs. dosimetry data collected via an in-reactor irradiation monitoring project.
- Correlation of a set of in-vessel surveillance data vs. GE-calculated results.
- Uncertainty and bias assessments.

For the past two decades, GE has provided services in the area of RPV fluence evaluations, using both calculations and dosimetry. The fluence calculation methodology employed by GE has been standardized in the past decade. The calculated ratio of the surveillance sample flux to the peak flux at RPV defines a lead factor. This lead factor is applied to the sample dosimetry data for determination of the RPV peak fluence, which is required for the vessel fracture toughness evaluations.

In order to comply with the provisions of RG 1.190 for a best-estimate fluence, GE has revised several aspects of the fluence evaluation processes. In the current method, the cross-section data for iron, oxygen, and hydrogen are updated with the ENDF/B-VI values. In addition, the material composition and geometric outline of the steel components in

[1] Evaluated Nuclear Data File (ENDF). See "ENDF/B Summary Documentation," BNL-NCS-17541 (ENDF-201), R, Kinsey, ed. (July 1979).

downcomer are explicitly modeled. Consequently, the current method provides more realistic neutron flux distributions in the RPV and its internal components.

2.0 GE METHODOLOGY

For the evaluation of RPV fast neutron flux, GE has traditionally employed the flux synthesis technique where a combination of two-dimensional calculations are performed and the results combined to synthesize a three-dimensional flux distribution.

The two-dimensional code used by GE is DORTG01V, which is a discrete ordinates code package based on CCC-543 TORT-DORT Version 2.8.14 issued by Oak Ridge National Laboratory (ORNL) in 1984[3]. DORTG01V is a controlled code in the GE Engineering Computer Program (ECP) library[1].

2.1 DISCRETE ORDINATES METHOD

2.1.1 (r,θ) Model

[1] ECP library contains controlled computer codes and cross section libraries approved for design applications.

In the angular coordinate, θ, the mesh size is $^1/_2$ degree or less per mesh step. Mesh size in the radial direction varies with each region. Generally, a fine mesh is provided near material interfaces, where significant flux gradients are expected. Fine meshes are also applied near the capsule, the RPV clad, and the innermost portion of the RPV. Sufficient fine mesh steps are provided to simulate the outer profile of the core. The mesh step is fine enough such that the (r,θ) representation would reproduce the true physical bundle area to within ~0.5%.

2.1.2 (r,z) Model

2.1.3 Coolant Density

2.1.4 Neutron Source Distribution

The spatial distribution of neutron source density is assumed to be proportional to the relative cycle-averaged energy production at each fuel node and each bundle location. A typical core-averaged relative power density variation is shown in Table 2-2 for (r,θ) calculation. A typical core-zone averaged variation in the axial direction is shown in Table 2-3 for (r,z) calculation.

2.1.5 Material Compositions

The composition in each material zone is treated as a homogenized mixture. The volume fractions of solid material and coolant in the core regions are calculated based on the bundle design data.

2.1.6 Cross-Section Library

The cross-section data used in the DORT calculation are processed with the nuclear cross-section processing package in the GE ECP library. The basic cross-section library used is the MATXS library[5], which was generated by Los Alamos National Laboratory for reactor physics application[5]. The MATXS library contains the 80-group infinite dilute neutron cross sections for various temperatures and self-shielding parameters (σ_o). This library is used in performing the resonance self-shielding, spatial self-shielding, elastic removal correction, reactor and cell flux solutions, and cross-section condensation to fewer groups.

The nuclide atom densities described in Sections 2.1.3 and 2.1.5 are incorporated, in conjunction with the microscopic cross section set, to create the macroscopic mixture cross sections which approximate the anisotropic scattering cross sections with 3rd-order Legendre polynomial expansions (P3). These data sets are further transformed to a group-organized format compatible with the DORT inputs.

2.1.7 Results of Discrete Ordinates Method

Figure 2-3 shows an example of the calculated fast neutron flux (E>1MeV) vs. azimuth along the reactor shroud inner radius. Figure 2-4 shows the axial flux profile and the elevation of peak flux on the same radius.

2.2 CURRENT VS. TRADITIONAL METHODOLOGIES

2.3 MONTE-CARLO TECHNIQUE

Table 2-1
Sample Nodal Coolant Density

	Coolant Density (g/cc)				
Node	R1	R2	R3	R4	Core Average
25	0.4429	0.3902	0.3635	0.3657	0.3896
24	0.4454	0.3920	0.3652	0.3680	0.3917
23	0.4497	0.3948	0.3679	0.3714	0.3949
22	0.4552	0.3984	0.3714	0.3759	0.3992
21	0.4618	0.4028	0.3757	0.3813	0.4043
20	0.4692	0.4080	0.3807	0.3872	0.4101
19	0.4774	0.4137	0.3864	0.3928	0.4164
18	0.4864	0.4201	0.3926	0.3992	0.4233
17	0.4963	0.4272	0.3994	0.4065	0.4311
16	0.5155	0.4472	0.4202	0.4272	0.4513
15	0.5267	0.4554	0.4279	0.4355	0.4600
14	0.5390	0.4643	0.4362	0.4446	0.4696
13	0.5543	0.4755	0.4467	0.4562	0.4817
12	0.5716	0.4886	0.4590	0.4696	0.4956
11	0.5907	0.5039	0.4736	0.4854	0.5117
10	0.6115	0.5216	0.4909	0.5038	0.5302
9	0.6336	0.5421	0.5114	0.5253	0.5513
8	0.6567	0.5657	0.5355	0.5506	0.5753
7	0.6802	0.5931	0.5641	0.5802	0.6026
6	0.7031	0.6250	0.5979	0.6148	0.6335
5	0.7242	0.6619	0.6381	0.6547	0.6682
4	0.7408	0.7016	0.6839	0.6971	0.7048
3	0.7500	0.7369	0.7282	0.7346	0.7370
2	0.7535	0.7526	0.7514	0.7522	0.7524
1	0.7552	0.7552	0.7552	0.7552	0.7552

Table 2-2
Sample Bundle Relative Power Density

I\J	1	2	3	4	5	6	7	8	9	10	11
1	1.2147	1.4181	1.3014	1.3900	1.2992	1.5350	1.3712	1.4265	1.1662	1.0239	0.5845
2	1.3896	1.3202	1.4103	1.3801	1.4863	1.4536	1.4978	1.2650	1.2915	0.9654	0.5434
3	1.2649	1.4028	1.2828	1.4728	1.3410	1.5163	1.3296	1.3524	1.2156	0.8058	0.4865
4	1.3796	1.3772	1.4720	1.3713	1.4449	1.4094	1.4058	1.3133	0.9378	0.6598	
5	1.2975	1.4848	1.3407	1.4462	1.2752	1.4106	1.1927	1.1810	0.7944		
6	1.5363	1.4559	1.5186	1.4149	1.4152	1.1538	1.1898	1.0263	0.6002		
7	1.3728	1.5000	1.3332	1.4120	1.1982	1.1914	0.9299	0.7586	0.4949		
8	1.4283	1.2667	1.3549	1.3171	1.1842	1.0267	0.7580	0.5497			
9	1.1655	1.2943	1.2184	0.9396	0.8044	0.5975	0.4899				
10	1.0298	0.9695	0.8084	0.6643							
11	0.6196	0.5525	0.4911								

Table 2-3
Sample Normalized Power Density

Node	R1	R2	R3	R4	Core Avg
25	0.1125	0.1663	0.2348	0.2911	0.2007
24	0.3051	0.4136	0.5431	0.6729	0.4820
23	0.4059	0.5644	0.7327	0.8921	0.6471
22	0.4752	0.6971	0.8963	1.0698	0.7835
21	0.5185	0.7945	1.0122	1.1827	0.8768
20	0.5461	0.8654	1.0918	1.2381	0.9365
19	0.5637	0.9163	1.1451	1.2359	0.9686
18	0.5754	0.9546	1.1819	1.2319	0.9909
17	0.5831	0.9864	1.2101	1.2329	1.0092
16	0.5698	0.9857	1.2050	1.2010	0.9974
15	0.5783	1.0177	1.2333	1.2138	1.0185
14	0.6627	1.1353	1.3764	1.3440	1.1384
13	0.6759	1.1749	1.4119	1.3708	1.1677
12	0.6861	1.2161	1.4514	1.3997	1.1983
11	0.6914	1.2520	1.4840	1.4206	1.2227
10	0.6933	1.2841	1.5094	1.4332	1.2414
9	0.6929	1.3124	1.5205	1.4304	1.2510
8	0.6884	1.3432	1.5414	1.4390	1.2656
7	0.6802	1.3750	1.5608	1.4510	1.2799
6	0.6670	1.4050	1.5765	1.4625	1.2914
5	0.6463	1.4246	1.5865	1.4688	1.2956
4	0.6144	1.4107	1.5718	1.4483	1.2757
3	0.5645	1.3082	1.4754	1.3464	1.1878
2	0.4700	1.0270	1.1865	1.0735	0.9507
1	0.1683	0.3287	0.4093	0.3679	0.3225
Avg	0.5534	1.0144	1.2059	1.1967	1.0000

Table 2-4
Group Structure for 80-Group Neutron Cross-Section Data

Group Number	Upper Energy (eV)	Lethargy Width	Group Number	Upper Energy (eV)	Lethargy Width
1	2.0000E+7	0.168	41	1.5034E+4	0.125
2	1.6905E+7	0.125	42	1.3268E+4	0.125
3	1.4918E+7	0.100	43	1.1709E+4	0.125
4	1.3499E+7	0.125	44	1.0333E+4	0.125
5	1.1912E+7	0.175	45	9.1188E+3	0.125
6	1.0000E+7	0.250	46	8.0473E+3	0.125
7	7.7880E+6	0.250	47	7.1017E+3	0.125
8	6.0653E+6	0.250	48	6.2673E+3	0.125
9	4.7237E+6	0.250	49	5.5308E+3	0.125
10	3.6788E+6	0.250	50	4.8810E+3	0.125
11	2.8650E+6	0.250	51	4.3074E+3	0.125
12	2.2313E+6	0.250	52	3.8013E+3	0.125
13	1.7377E+6	0.250	53	3.3546E+3	0.125
14	1.3534E+6	0.125	54	2.9604E+3	0.125
15	1.1943E+6	0.125	55	2.6126E+3	0.125
16	1.0540E+6	0.125	56	2.3056E+3	0.125
17	9.3014E+5	0.125	57	2.0347E+3	0.125
18	8.2085E+5	0.125	58	1.7956E+3	0.125
19	7.2440E+5	0.125	59	1.5846E+3	0.125
20	6.3928E+5	0.125	60	1.3984E+3	0.125
21	5.6416E+5	0.125	61	1.2341E+3	0.125
22	4.9787E+5	0.125	62	1.0891E+3	0.125
23	4.3937E+5	0.125	63	9.6112E+2	0.250
24	3.8774E+5	0.250	64	7.4852E+2	0.250
25	3.0197E+5	0.250	65	5.8295E+2	0.250
26	2.3518E+5	0.250	66	4.5400E+2	0.250
27	1.8316E+5	0.250	67	3.5358E+2	0.250
28	1.4264E+5	0.250	68	2.7536E+2	0.500
29	1.1109E+5	0.250	69	1.6702E+2	0.500
30	8.6517E+4	0.250	70	1.0130E+2	0.500
31	6.7380E+4	0.250	71	6.1442E+1	0.500
32	5.2475E+4	0.250	72	3.7266E+1	0.500
33	4.0868E+4	0.250	73	2.2603E+1	0.500
34	3.1828E+4	0.125	74	1.3710E+1	0.500
35	2.8088E+4	0.075	75	8.3153E+0	0.500
36	2.6058E+4	0.050	76	5.0435E+0	0.500
37	2.4788E+4	0.125	77	3.0590E+0	1.000
38	2.1875E+4	0.125	78	1.1253E+0	1.000
39	1.9304E+4	0.125	79	4.1399E-1	1.000
40	1.7036E+4	0.125	80	1.5230E-1	7.000
			Minimum	1.3888E-4	

Table 2-5
Group Structure for 26-Group Neutron Cross-Section Data

Figure 2-1. Schematic View of (r, θ) Model

Figure 2-2. Schematic View of (r, z) Model

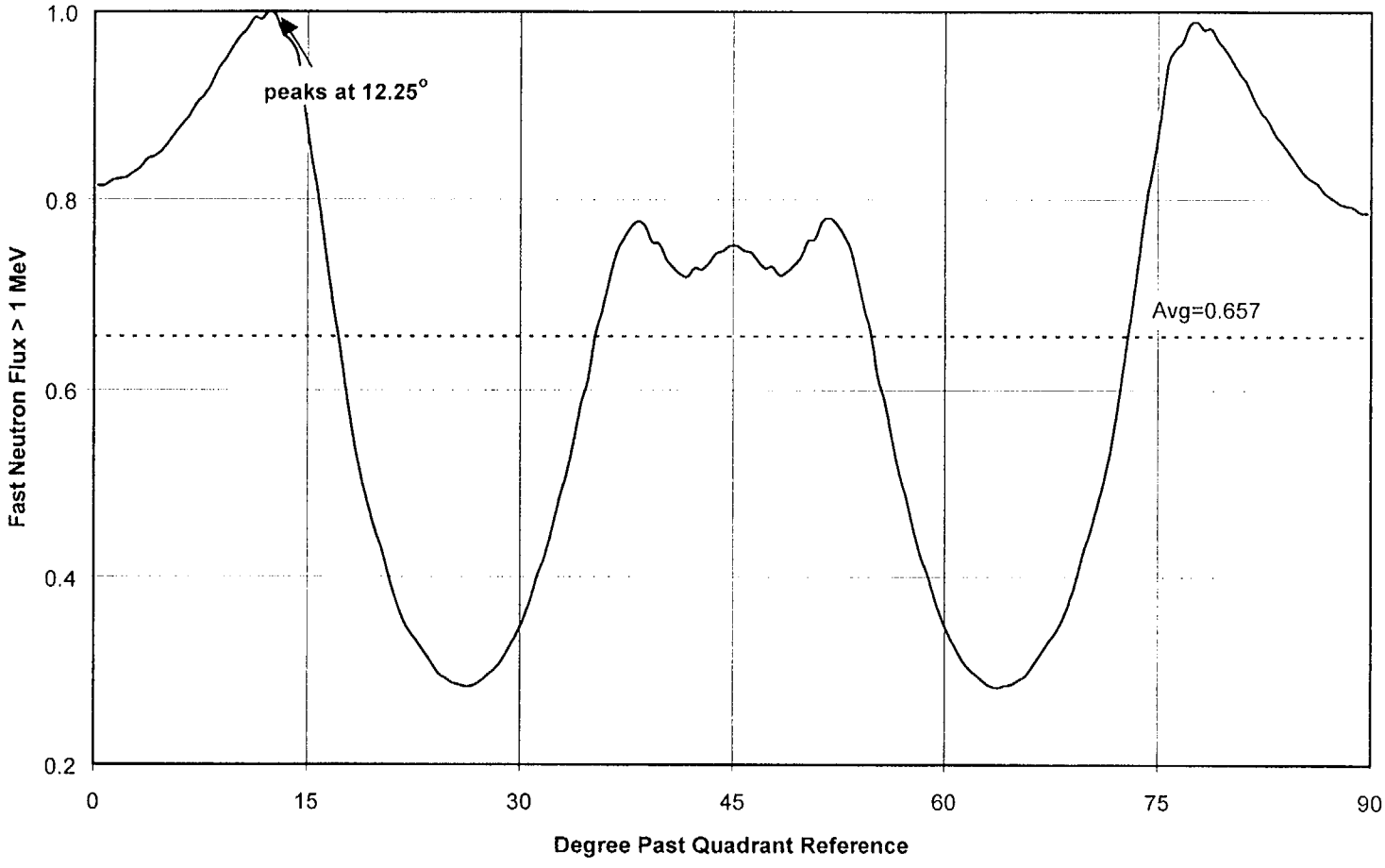

Figure 2-3. Sample Relative Neutron Flux (E>1 MeV) vs. Azimuth at Shroud ID

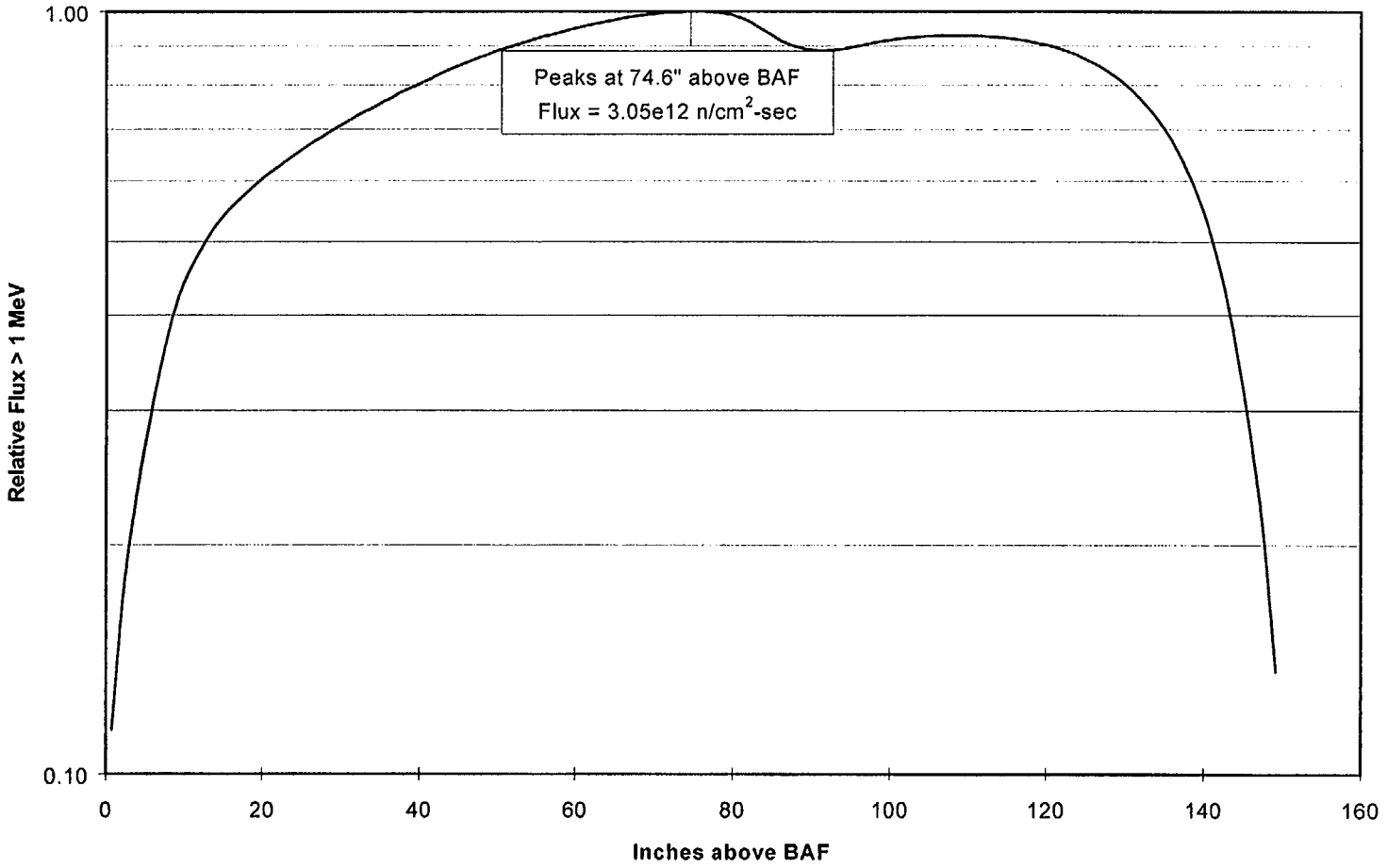

Figure 2-4. Sample Relative Neutron Flux (E>1 MeV) vs. Axial Elevation at Shroud ID

3.0 GE SOLUTIONS TO BWR BENCHMARK PROBLEM

This section documents the GE discrete ordinates solutions to the BWR benchmark problem as defined in NUREG/CR-6115, which was published by Brookhaven National Laboratory (BNL) for the NRC as one of the benchmarks for validating fluence calculation methodologies.

The solution provided in NUREG/CR-6115 (herein called the BNL solution) determines the RPV flux by combining the results of DORT(r,θ), DORT(r,z), and DORT(r) calculations. The GE solution to the same benchmark problem, using similar discrete ordinates methodology is described below.

3.1 GE SOLUTION USING DISCRETE ORDINATES METHOD

3.1.1 Core Configuration

The benchmark problem is modeled for a BWR core with 800 fuel bundles. The active core height is 381 cm. The core configuration, including radii of various material regions, are described in Figures 3-1 and 3-2 for the (r,θ) and (r,z) calculations, respectively. The RPV has an inner radius of 321.786 cm and is 16.129 cm thick, with a 0.476 cm stainless steel liner on the inner surface.

The (r,θ) calculation models the core and outward surroundings including the shroud, jet pumps and risers, the RPV, and an outer concrete biological shield. To be consistent with the BNL solution edits, where the RPV peak flux occurs at elevation 306.605 cm, the (r,θ) calculation model is selected at the same elevation.

In addition to the components modeled in the (r,θ) calculation, the (r,z) calculation models the core inlet and core plate which are below the active fuel region as well as upper reflector, top guide, and steam separator, which are above the core. The (r,z) calculation model is chosen to simulate the core dimension at 40.24° azimuth where the maximum core radius occurs.

Table 3-1 shows the radial, axial, and azimuthal meshes used in the GE DORT(r,θ) and (r,z) calculations. These data are almost identical to those in Table 4.2.2.1 of NUREG/CR-6115. The only exceptions are the inner and outer radii of the shroud, which were listed incorrectly in NUREG/CR-6115. Hence, GE made the necessary corrections to these data. Similarly, radial meshes near the capsule were modified slightly in order to account for the inner surface as well as the centerline of the capsule.

3.1.2 Power Distribution

In the benchmark problem, the assumed bundle power and exposure simulated those of an equilibrium core. The relative power of each fuel bundle was given in Table 2.2.2.4 of NUREG/CR-6115. These relative powers had been rearranged and re-normalized so that the average power of a single bundle is one, as shown in Table 3-2. Since Table 3-2 shows a quadrant of the core, the values of diagonal bundles have been doubled from those in NUREG/CR-6115 to account for the actual relative power.

NUREG/CR-6115 also provided the nodal relative power in the axial direction. The core power distribution consists of three radial zones. For example, at elevation 306.605 cm (axial zone 18) the nodal power in the outermost layer is 0.0516 (or 1.29 times the core average, which is 0.04). The second layer is 0.0484 (1.21 times core average), and the inner core region is 0.0441 (1.1025 times core average). Since the DORT(r,θ) calculation is performed at 306.605 cm, these axial factors are multiplied by the relative power density in Table 3-2. The resulting data are listed in Table 3-3.

To simulate the BNL solution, one set of GE (r,θ) solutions also assumes a pin-by-pin or 8x8 power grid for each bundle at the outermost row, a 4x4 power grid for each second tier bundle, and 2x2 power grid for each third tier bundle. The remaining core regions are assumed to have uniform power density within the bundle. A second set of GE solution takes the traditional GE approach of assuming bundle-average power for inner core as well as for peripheral bundles. The end results of these two sets of solution will be compared to justify the calculation bias.

The axial power distribution for the (r,z) calculation combines the radial zone-average of Table 3-2 with the normalized axial power given in Table 2.2.2.6 of NUREG/CR-6115. The resulting power density map used for the actual calculation is shown in Table 3-4.

3.1.3 Material Composition and Coolant Density

The BWR benchmark problem assumes that each of the 800 fuel bundles consists of 62 fuel rods plus 2 water rods. The fuel channel thickness is 0.3048 cm, channel OD is 13.8557 cm. The assembly pitch is 15.24 cm (6") and fuel pin pitch is 1.61544 cm.

These volume fractions were used to generate the weighted atom density for each of the inner and outer core zones. The results are listed in Table 3-5. The downcomer is modeled in three different ways and details of which are addressed in Section 3.1.6.

3.1.4 Cross-Section Processing

Nuclear cross-section data processing in the GE discrete ordinates method has been described in Section 2.1.6. The atom densities of Table 3-5 are used as the basis for generating macroscopic cross sections for the DORT calculations.

The isotopic fractions of these isotopes, 5.9%, 91.72%, 2.1%, and 0.28%, respectively, are taken from the "Nuclides and Isotopes"[6].

3.1.5 Neutron Source Calculation

A fixed source distribution proportional to the power density is assumed for the neutron source. Since the actual neutron source strength was not provided in NUREG/CR-6115, GE performed a lattice depletion calculation with an assumed 8x8 array fuel of 3.78% average enrichment.

where

3833 MWt is the thermal power level.

0.125 represents 1/8th of the core.

381 cm is the total height of the active core.

For the (r,z) calculation, the goal is to generate a relative, rather than absolute, flux magnitude. Therefore a precise neutron source description is not essential. A typical number of 1.0E20 n/sec was used as the fixed source input for the calculation.

3.1.6 Treatment of Downcomer Region

Precise modeling of the BWR downcomer components and materials is not practical in a two-dimensional calculation. In order to assess the effect of neutron interactions in the downcomer, three variations of downcomer model were used in the GE solutions of (r,θ) calculations.

The first model treats the downcomer region as composed solely of subcooled water, without any metal components. This is a conservative approach traditionally employed by GE.

The second model assumes that the downcomer is a homogenized mixture of coolant and metal, the effective neutron scattering by steel is accounted for to a certain extent.

The third model considers the downcomer as composed of heterogeneous material zones, with each jet pump and riser as individual component.

The results of these three downcomer models are presented in the next section and in Section 3.2 as part of the sensitivity studies.

For the (r,z) calculation, the second model is used to simulate the material compositions in the downcomer region.

3.1.7 GE Discrete Ordinates Solution Results

GE calculated flux results (E>1 MeV) using the discrete ordinates method described above are presented in the following figures:

Figure 3-3	Downcomer Flux with Various Downcomer Models
Figure 3-4	RPV ID Flux with Various Downcomer Models
Figure 3-5	RPV 1/4T Flux with Various Downcomer Models
Figure 3-6	RPV T Flux with Various Downcomer Models
Figure 3-7	Axial Flux Profile at Various Radial Locations
Figure 3-8	GE vs. BNL Azimuthal Flux Profile at Downcomer
Figure 3-9	GE vs. BNL Azimuthal Flux Profile at RPV ID
Figure 3-10	GE vs. BNL Flux Spectra at RPV ID
Figure 3-11	GE vs. BNL Flux Spectra at RPV 1/2T
Figure 3-12	GE vs. BNL Flux Spectra at Capsule

The extracted edits are listed in Table 3-6, together with the results of the sensitivity studies described in Section 3.2. As mentioned in Section 3.1.2, the pin-by-pin power densities are used for the three downcomer models. A fourth calculation was performed to validate the current GE methodology. This calculation uses the bundle-average power in conjunction with the third downcomer model and is designated Case 4 in Table 3-6. Results of Case 4 are used as the basis of comparison for all other cases.

Case 6 simulates the traditional model employed by GE, except it uses ENDF/B-VI library instead of the ENDF/B-V library. The over-prediction of vessel ID peak flux by this model should be less than 17% (difference between Case 6 and BNL minus Case 9). As stated above, for BWRs with different configurations, the over-prediction should be less if the locations of jet pumps are not coincident with the peak flux azimuth.

The calculation model of Case 3 is almost identical to that of BNL solution. Consequently, the peak vessel ID flux is within 0.5% of the BNL result.

Comparisons between the results of current GE methodology and BNL solution are presented in Figures 3-8 through 3-12. Along the circumference of the RPV inner surface, the two solutions

differ by less than 10%. However, both solutions predicted the same peak flux locations at 42.5°.

3.1.8 Flux >0.1 MeV

Figures 3-13 and 3-14 present the comparison between the GE and BNL solutions for the >0.1 MeV fluxes at the downcomer and RPV ID, respectively. The differences between the two solutions are consistent with those displayed in Figures 3-8 and 3-9 for neutron flux above 1 MeV.

3.2 SENSITIVITY STUDIES

Sensitivity studies of variables in the discrete ordinates calculations were performed and the effect of each variable is assessed. The study results are summarized in Table 3-6. The most significant among these variables is the treatment of downcomer components, which was discussed in the previous section. Overestimation of vessel flux due to omission of steel components in downcomer is especially prominent if the flux peaks at locations shielded by a jet pump or riser component, as is the case here.

The following figures demonstrate the effects of calculation variables such as cross section library, pin-by-pin power distribution, and angular quadratures:

Figure 3-15	ENDF/B-VI vs. ENDF/B-V Flux at RPV ID
Figure 3-16	ENDF/B-VI vs. ENDF/B-V Flux at RPV 1/4T
Figure 3-17	ENDF/B-VI vs. ENDF/B-V Flux at RPV T
Figure 3-18	Pin-By-Pin vs. Bundle-Average Flux at Shroud ID
Figure 3-19	Pin-By-Pin vs. Bundle-Average Flux at RPV ID
Figure 3-20	S_{12} vs. S_8 Flux at Shroud ID
Figure 3-21	S_{12} vs. S_8 Flux at RPV ID

The results of a sensitivity study of the effects of cross section library on the fast neutron flux are presented in Table 3-7. The base case uses ENDF/B-V library (Case 7). Case 8 uses ENDF/B-V library overridden with ENDF/B-VI iron cross sections. Case 9 uses ENDF/B-V library overridden with ENDF/B-VI iron, oxygen, and hydrogen cross sections. The calculation model for this study is consistent within the study group, however it is slightly different from those of Table 3-6. Therefore, the comparisons are only made within the group.

The effect of pin-by-pin power vs bundle-average power is demonstrated through Figures 3-18 and 3-19, and Table 3-6.

When this effect is taken into consideration, the traditional GE method produces a flux value almost identical to the BNL result in the downcomer near the shroud outer surface, as indicated in Table 3-6 Case 6.

Angular quadrature higher than S_8 produces less than 1% change in the calculated flux, as shown in Figures 3-20 and 3-21 as well as Table 3-6 Case 3a. This conclusion is consistent with that provided by Table 3.4.2 of NUREG/CR-6115.

Using a reflective boundary condition to approximate the innermost core region provides almost identical flux results as a full core model, as demonstrated in Table 3-6 Case 5. This is further proof that the traditional practice adopted by GE to economize computational effort did not sacrifice the accuracy of calculated flux.

3.3 CONCLUSIONS

GE solutions to the BWR benchmark problem were performed using the GE controlled version of the DORT code, with various calculation models simulating the peripheral bundle powers and downcomer material compositions.

In the downcomer near the outer surface of the shroud, GE and BNL solutions produce almost identical flux results.

The methodology traditionally employed by GE produces peak vessel flux approximately 16% higher than the BNL result, due to the placement of jet pump riser which coincides with the peak flux azimuth. With the same method, when the conservatism created by bundle-average power is excluded, the traditional GE approach and BNL solution produce almost identical flux results in the downcomer near the outer surface of the shroud.

Table 3-1
Meshes for DORT Calculations

Node	R (cm)	Z (cm)	θ (revolution)
1	0.00000	0.00000	0.00000E+00
2	7.50000	3.09750	6.24722E-03
3	15.0000	6.19500	7.63889E-03
4	22.5000	9.29250	9.02778E-03
5	30.0000	12.3900	1.04194E-02
6	37.5000	15.4767	1.37889E-02
7	45.0000	18.5633	1.53167E-02
8	52.5000	21.6500	1.79556E-02
9	60.0000	24.7367	1.95444E-02
10	67.5000	27.8233	2.00389E-02
11	75.0000	30.9100	2.06556E-02
12	82.5000	33.9967	2.15389E-02
13	90.0000	37.0833	2.36278E-02
14	97.5000	40.1700	2.37944E-02
15	105.000	43.2567	2.47944E-02
16	112.500	46.3433	2.63556E-02
17	120.000	49.4300	3.06500E-02
18	127.500	52.4780	3.39278E-02
19	135.000	55.5260	3.89833E-02
20	142.500	58.5740	4.15722E-02
21	150.000	61.6220	4.45389E-02
22	157.500	64.6700	4.71278E-02
23	165.000	67.7180	4.94056E-02
24	172.500	70.7660	5.26833E-02
25	180.000	73.8140	5.56500E-02
26	182.602	76.8620	5.67889E-02
27	185.560	79.9100	6.12056E-02
28	186.709	82.9580	6.37944E-02
29	187.785	86.0060	6.67611E-02
30	188.896	89.0540	6.80222E-02
31	189.782	92.1020	6.88444E-02
32	190.616	95.1500	7.01389E-02
33	191.625	98.1980	7.16222E-02
34	192.706	101.246	7.21278E-02
35	193.369	104.294	7.54611E-02
36	194.008	107.342	7.76833E-02
37	194.782	110.390	7.95444E-02
38	195.444	113.438	8.04611E-02
39	196.207	116.486	8.20389E-02
40	198.098	119.534	8.32111E-02
41	198.825	122.582	8.48778E-02
42	199.580	125.630	8.60167E-02
43	200.562	128.678	8.75944E-02

Table 3-1
Meshes for DORT Calculations (Continued)

Node	R (cm)	Z (cm)	θ (revolution)
44	201.416	131.726	8.80056E-02
45	202.458	134.774	9.03722E-02
46	203.446	137.822	9.29611E-02
47	204.500	140.870	9.42056E-02
48	205.506	143.918	9.71278E-02
49	206.520	146.966	9.86445E-02
50	207.440	150.014	1.01506E-01
51	208.610	153.062	1.05650E-01
52	209.491	156.110	1.09689E-01
53	210.474	159.158	1.11206E-01
54	211.606	162.206	1.12328E-01
55	212.585	165.254	1.15372E-01
56	213.795	168.302	1.17356E-01
57	214.611	171.350	1.18811E-01
58	215.643	174.398	1.22222E-01
59	216.308	177.446	1.23611E-01
60	217.732	180.494	1.24861E-01
61	218.318	183.542	1.25000E-01
62	219.483	186.590	
63	220.282	189.638	
64	221.543	192.686	
65	222.394	195.734	
66	223.735	198.782	
67	225.048	201.830	
68	226.423	204.878	
69	227.237	207.926	
70	228.431	210.974	
71	229.450	214.022	
72	230.719	217.070	
73	231.344	202.118	
74	232.630	223.116	
75	233.895	226.214	
76	234.874	229.262	
77	235.625	232.310	
78	236.176	235.430	
79	237.228	238.430	
80	238.470	241.430	
81	239.300	244.430	
82	240.227	247.550	
83	240.783	250.598	
84	241.970	253.646	
85	242.570	256.694	
86	243.672	259.742	

Table 3-1
Meshes for DORT Calculations (Continued)

Node	R (cm)	Z (cm)	θ (revolution)
87	244.461	262.790	
88	244.974	265.838	
89	245.616	268.886	
90	247.540	271.934	
91	248.091	274.982	
92	249.019	278.030	
93	250.597	281.078	
94	251.148	284.126	
95	252.568	287.174	
96	252.267	290.222	
97	254.077	293.270	
98	255.598	297.080	
99	257.727	300.890	
100	258.519	304.700	
101	259.530	308.510	
102	260.326	310.430	
103	261.122	313.430	
104	261.918	316.430	
105	262.715	319.430	
106	263.511	323.750	
107	264.307	326.798	
108	265.103	329.846	
109	265.899	332.894	
110	266.695	335.942	
111	267.491	338.990	
112	268.288	344.070	
113	269.557	349.150	
114	270.288	354.230	
115	272.098	359.310	
116	273.367	364.390	
117	274.073	369.470	
118	274.778	374.550	
119	275.368	379.630	
120	276.189	384.710	
121	276.895	389.790	
122	277.600	394.870	
123	278.600	399.950	
124	278.878	405.030	
125	279.627	410.110	
126	280.376	415.190	
127	281.125	420.270	
128	281.875	425.350	

Table 3-1
Meshes for DORT Calculations (Continued)

Node	R (cm)	Z (cm)	θ (revolution)
129	282.624	430.430	
130	283.454	436.603	
131	284.284	442.777	
132	285.114	448.950	
133	285.944	455.123	
134	286.774	461.297	
135	287.604	467.470	
136	288.435	473.643	
137	289.265	479.817	
138	290.095	485.990	
139	290.925	495.637	
140	291.755	505.284	
141	292.585	514.931	
142	293.415	524.578	
143	294.245	534.225	
144	295.075	543.872	
145	295.905	553.519	
146	296.735	563.166	
147	297.565	572.814	
148	298.396	582.461	
149	299.226	592.108	
150	300.056	601.755	
151	300.886	611.402	
152	301.716	621.049	
153	302.546	630.696	
154	303.376	640.343	
155	304.125	649.990	
156	304.875	659.637	
157	305.624	669.284	
158	306.373	678.931	
159	307.122	688.578	
160	307.919	698.225	
161	308.716	707.872	
162	309.513	717.519	
163	310.310	727.166	
164	311.156	736.813	
165	312.002	746.461	
166	312.848	756.108	
167	313.695	765.755	
168	314.541	775.402	
169	315.387	785.049	
170	316.233	794.696	

Table 3-1
Meshes for DORT Calculations (Continued)

Node	R (cm)	Z (cm)	θ (revolution)
171	317.079	804.343	
172	317.925	813.990	
173	318.772		
174	319.618		
175	320.464		
176	321.310		
177	321.786		
178	322.786		
179	324.500		
180	325.318		
181	326.318		
182	327.834		
183	329.351		
184	330.351		
185	331.867		
186	333.383		
187	334.383		
188	336.149		
189	337.915		
190	340.790		
191	346.290		
192	351.790		
193	351.949		
194	354.806		
195	357.663		
196	360.520		
197	365.611		
198	370.701		
199	375.792		
200	380.883		
201	385.973		
202	391.064		
203	396.155		
204	401.245		
205	406.336		
206	411.427		
207	416.517		
208	421.608		
209	426.699		
210	431.789		

Table 3-1
Meshes for DORT Calculations (Continued)

Node	R (cm)	Z (cm)	θ (revolution)
211	436.880		
212	437.500		
213	441.500		
214	445.500		
215	449.500		
216	453.500		
217	457.500		
218	461.500		
219	465.500		
220	469.500		
221	473.500		
222	477.500		

Table 3-2
BWR Benchmark Problem Bundle Power Density

	1	2	3	4	5	6	7	8	9	10	11	12	13	14	15	16
1	1.007	1.074	1.058	1.114	1.101	1.107	1.356	1.082	1.08	1.076	1.317	1.063	1.192	0.82	0.602	0.326
2	1.074	1.292	1.122	1.333	1.108	1.358	1.116	1.323	1.078	1.319	1.096	1.288	0.991	0.999	0.587	0.32
3	1.058	1.122	1.125	1.114	1.36	1.128	1.344	1.087	1.109	1.105	1.33	1.058	1.173	0.791	0.542	
4	1.114	1.333	1.114	1.346	1.101	1.331	1.089	1.117	1.098	1.34	1.098	1.27	0.968	0.94	0.471	
5	1.101	1.108	1.36	1.101	1.094	1.083	1.106	1.096	1.344	1.109	1.318	1.041	1.122	0.735	0.438	
6	1.107	1.358	1.128	1.331	1.083	1.325	1.102	1.341	1.114	1.328	1.065	1.205	0.898	0.836	0.392	
7	1.356	1.116	1.344	1.089	1.106	1.102	1.343	1.101	1.325	1.079	1.24	0.947	0.971	0.586	0.327	
8	1.082	1.323	1.087	1.117	1.096	1.341	1.101	1.083	1.068	1.251	0.979	1.037	0.668	0.428		
9	1.08	1.078	1.109	1.098	1.344	1.114	1.325	1.068	1.25	0.997	1.079	0.739	0.484			
10	1.076	1.319	1.105	1.34	1.109	1.328	1.079	1.251	0.997	0.544	0.781	0.605	0.361			
11	1.317	1.096	1.33	1.098	1.318	1.065	1.24	0.979	1.079	0.781	0.629	0.462	0.265			
12	1.063	1.288	1.058	1.27	1.041	1.205	0.947	1.037	0.739	0.605	0.462	0.32				
13	1.192	0.991	1.173	0.968	1.122	0.898	0.971	0.668	0.484	0.361	0.265					
14	0.82	0.999	0.791	0.94	0.735	0.836	0.586	0.428								
15	0.602	0.587	0.542	0.471	0.438	0.392	0.327									
16	0.326	0.32														

Average

R1	1.1346
R2	0.6864
R3	0.3926

Table 3-3
Power Density at Elevation z=306.6 cm for DORT(r,θ) Calculation

I\J	1	2	3	4	5	6	7	8	9	10	11	12	13	14	15	16
1	1.1103	1.1835	1.1662	1.2279	1.2135	1.2207	1.4953	1.1926	1.1901	1.1866	1.4514	1.1715	1.3137	0.9042	0.7279	0.4211
2	1.1835	1.4248	1.2367	1.4693	1.2220	1.4976	1.2308	1.4590	1.1886	1.4544	1.2081	1.4197	1.0929	1.1016	0.7102	0.4129
3	1.1662	1.2367	1.2405	1.2279	1.4994	1.2432	1.4822	1.1984	1.2229	1.2183	1.4659	1.1661	1.2937	0.9574	0.6989	
4	1.2279	1.4693	1.2279	1.4841	1.2136	1.4669	1.2006	1.2314	1.2101	1.4778	1.2105	1.3998	1.0673	1.1379	0.6080	
5	1.2135	1.2220	1.4994	1.2136	1.2056	1.1942	1.2195	1.2081	1.4815	1.2225	1.4525	1.1479	1.2371	0.8889	0.5647	
6	1.2207	1.4976	1.2432	1.4669	1.1942	1.4611	1.2144	1.4783	1.2281	1.4640	1.1745	1.3288	0.9898	1.0117	0.5053	
7	1.4953	1.2308	1.4822	1.2006	1.2195	1.2144	1.4809	1.2133	1.4603	1.1897	1.3675	1.0444	1.0707	0.7096	0.4224	
8	1.1926	1.4590	1.1984	1.2314	1.2081	1.4783	1.2133	1.1942	1.1774	1.3791	1.0798	1.1435	0.8086	0.5523		
9	1.1901	1.1886	1.2229	1.2101	1.4815	1.2281	1.4603	1.1774	1.3777	1.0988	1.1898	0.8940	0.6245			
10	1.1866	1.4544	1.2183	1.4778	1.2225	1.4640	1.1897	1.3791	1.0988	0.6003	0.8611	0.7315	0.4653			
11	1.4514	1.2081	1.4659	1.2105	1.4525	1.1745	1.3675	1.0798	1.1898	0.8611	0.6940	0.5590	0.3422			
12	1.1715	1.4197	1.1661	1.3998	1.1479	1.3288	1.0444	1.1435	0.8940	0.7315	0.5590	0.4133				
13	1.3137	1.0929	1.2937	1.0673	1.2371	0.9898	1.0707	0.8086	0.6245	0.4653	0.3422					
14	0.9042	1.1016	0.9574	1.1379	0.8889	1.0117	0.7096	0.5523								
15	0.7279	0.7102	0.6989	0.6080	0.5647	0.5053	0.4224									
16	0.4211	0.4129														

Table 3-4
Power Density for (r,z) Calculation

Node	R1	R2	R3
1	0.0000	0.0000	0.0000
2	0.0144	0.0069	0.0039
3	0.0455	0.0211	0.0104
4	0.0564	0.0271	0.0133
5	0.0589	0.0295	0.0146
6	0.0574	0.0301	0.0150
7	0.0548	0.0302	0.0154
8	0.0525	0.0301	0.0157
9	0.0509	0.0302	0.0160
10	0.0499	0.0304	0.0164
11	0.0494	0.0307	0.0169
12	0.0490	0.0311	0.0174
13	0.0496	0.0316	0.0179
14	0.0500	0.0322	0.0185
15	0.0498	0.0327	0.0192
16	0.0505	0.0331	0.0196
17	0.0508	0.0334	0.0200
18	0.0500	0.0332	0.0203
19	0.0491	0.0328	0.0203
20	0.0488	0.0323	0.0199
21	0.0467	0.0309	0.0193
22	0.0424	0.0284	0.0181
23	0.0395	0.0256	0.0163
24	0.0332	0.0212	0.0136
25	0.0243	0.0155	0.0101
26	0.0103	0.0062	0.0044

Table 3-5
Material Compositions

Mixture	Element	# atom/b-cm
INNER CORE 1 (+WATER)	U-235	9.9196E-05
	U-238	5.3633E-03
	O (fuel)	1.0927E-02
	Zr	6.2833E-03
	H	3.0048E-02
	O	1.4269E-02
INNER CORE 2 (+WATER)	U-235	9.9196E-05
	U-238	5.3633E-03
	O (fuel)	1.0927E-02
	Zr	6.2833E-03
	H	2.7789E-02
	O	1.3894E-02
INNER CORE 3 (+WATER)	U-235	9.9196E-05
	U-238	5.3633E-03
	O (fuel)	1.0927E-02
	Zr	6.2833E-03
	H	2.2109E-02
	O	1.1054E-02
INNER CORE 4 (+WATER)	U-235	9.9196E-05
	U-238	5.3633E-03
	O (fuel)	1.0927E-02
	Zr	6.2833E-03
	H	1.8516E-02
	O	9.2576E-03
INNER CORE 5 (+WATER)	U-235	9.9196E-05
	U-238	5.3633E-03
	O (fuel)	1.0927E-02
	Zr	6.2833E-03
	H	1.6170E-02
	O	8.0849E-03
INNER CORE 6 (+WATER)	U-235	9.9196E-05
	U-238	5.3633E-03
	O (fuel)	1.0927E-02
	Zr	6.2833E-03
	H	1.4664E-02
	O	7.3319E-03
INNER CORE 7 (+WATER)	U-235	9.9196E-05
	U-238	5.3633E-03
	O (fuel)	1.0927E-02
	Zr	6.2833E-03
	H	1.3696E-02
	O	6.8478E-03

Table 3-5
Material Compositions (Continued)

Mixture	Element	# atom/b-cm
OUTER CORE 1 (+WATER)	U-235	9.9196E-05
	U-238	5.3633E-03
	O (fuel)	1.0927E-02
	Zr	6.2833E-03
	H	3.0048E-02
	O	1.5024E-02
OUTER CORE 2 (+WATER)	U-235	9.9196E-05
	U-238	5.3633E-03
	O (fuel)	1.0927E-02
	Zr	6.2833E-03
	H	3.0012E-02
	O	1.5006E-02
OUTER CORE 3 (+WATER)	U-235	9.9196E-05
	U-238	5.3633E-03
	O (fuel)	1.0927E-02
	Zr	6.2833E-03
	H	2.8166E-02
	O	1.4083E-02
OUTER CORE 4 (+WATER)	U-235	9.9196E-05
	U-238	5.3633E-03
	O (fuel)	1.0927E-02
	Zr	6.2833E-03
	H	2.4841E-02
	O	1.2421E-02
OUTER CORE 5 (+WATER)	U-235	9.9196E-05
	U-238	5.3633E-03
	O (fuel)	1.0927E-02
	Zr	6.2833E-03
	H	2.1441E-02
	O	1.0721E-02
OUTER CORE 6 (+WATER)	U-235	9.9196E-05
	U-238	5.3633E-03
	O (fuel)	1.0927E-02
	Zr	6.2833E-03
	H	1.9053E-02
	O	9.5266E-03
OUTER CORE 7 (+WATER)	U-235	9.9196E-05
	U-238	5.3633E-03
	O (fuel)	1.0927E-02
	Zr	6.2833E-03
	H	1.8042E-02
	O	9.0210E-03

Table 3-5
Material Compositions (Continued)

Mixture	Element	# atom/b-cm
Reflector Water	H	4.9284E-02
	O	2.4642E-02
Shroud	Fe	5.8300E-02
(SS-304)	Cr	1.7400E-02
	Ni	8.5500E-03
	Mn	1.5200E-03
	Si	8.9300E-04
	C	2.3700E-04
Downcomer Model 1	H	5.0455E-02
(Water only)	O	2.5228E-02
Downcomer Model 2	H	4.8801E-02
(Water +Jet Pump)	O	2.4401E-02
	Fe	2.0904E-03
	Ni	2.2599E-04
	Cr	5.0849E-04
RPV Liner	Fe	5.8300E-02
(SS-304)	Cr	1.7400E-02
	Ni	8.5500E-03
	Mn	1.5200E-03
	Si	8.9300E-04
	C	2.3700E-04
RPV Wall	Fe	8.1900E-02
(Steel)	Mn	1.1200E-03
	Ni	4.4400E-04
	Cr	1.2700E-04
	C	9.8100E-04
	Si	3.7100E-04
Cavity	O	9.6200E-06
insulation Liner	Fe	5.8300E-02
(SS-304)	Cr	1.7400E-02
	Ni	8.5500E-03
	Mn	1.5200E-03
	Si	8.9300E-04
	C	2.3700E-04

Table 3-5
Material Compositions (Continued)

Mixture	Element	# atom/b-cm
Insulation	Al	6.0603E-03
Cavity	O	9.6200E-06
Concrete Wall	Fe	6.0976E-04
	H	1.5137E-02
	C	2.2403E-04
	O	8.5327E-02
	Na	2.0455E-03
	Mg	2.8832E-04
	Al	4.6560E-03
	Si	3.0778E-02
	K	1.3500E-03
	Ca	4.4612E-03
Inlet Region	H	3.5415E-02
	O	1.7708E-02
	Zr	7.9747E-03
	Cr	1.9749E-03
	Mn	1.7252E-04
	Fe	6.6171E-03
	Ni	9.7043E-04
	Si	1.0136E-04
	C	2.6900E-05
Core Plate	H	4.6642E-02
	O	2.3321E-02
	Cr	1.3154E-03
	Mn	1.1491E-04
	Fe	4.4075E-03
	Ni	6.4638E-04
	Si	6.7511E-05
	C	1.7917E-05
Top	H	1.2153E-02
	O	6.0767E-03
	Zr	7.6896E-03
Upper Reflector	H	9.8223E-03
	O	4.9112E-03
	Zr	7.5125E-03
	Cr	2.8153E-03
	Mn	2.4594E-04
	Fe	9.4329E-03
	Ni	1.3834E-04
	Si	1.4449E-04
	C	3.8347E-05
Steam Separater	H	1.4785E-02
	O	7.3926E-03

Table 3-6
Sensitivity of DORT Calculated Flux (E>1MeV) to Input Parameters

Table 3-7
Sensitivity of Varying Cross Section Library on Flux at 44.97°

BWR PLANAR GEOMETRY

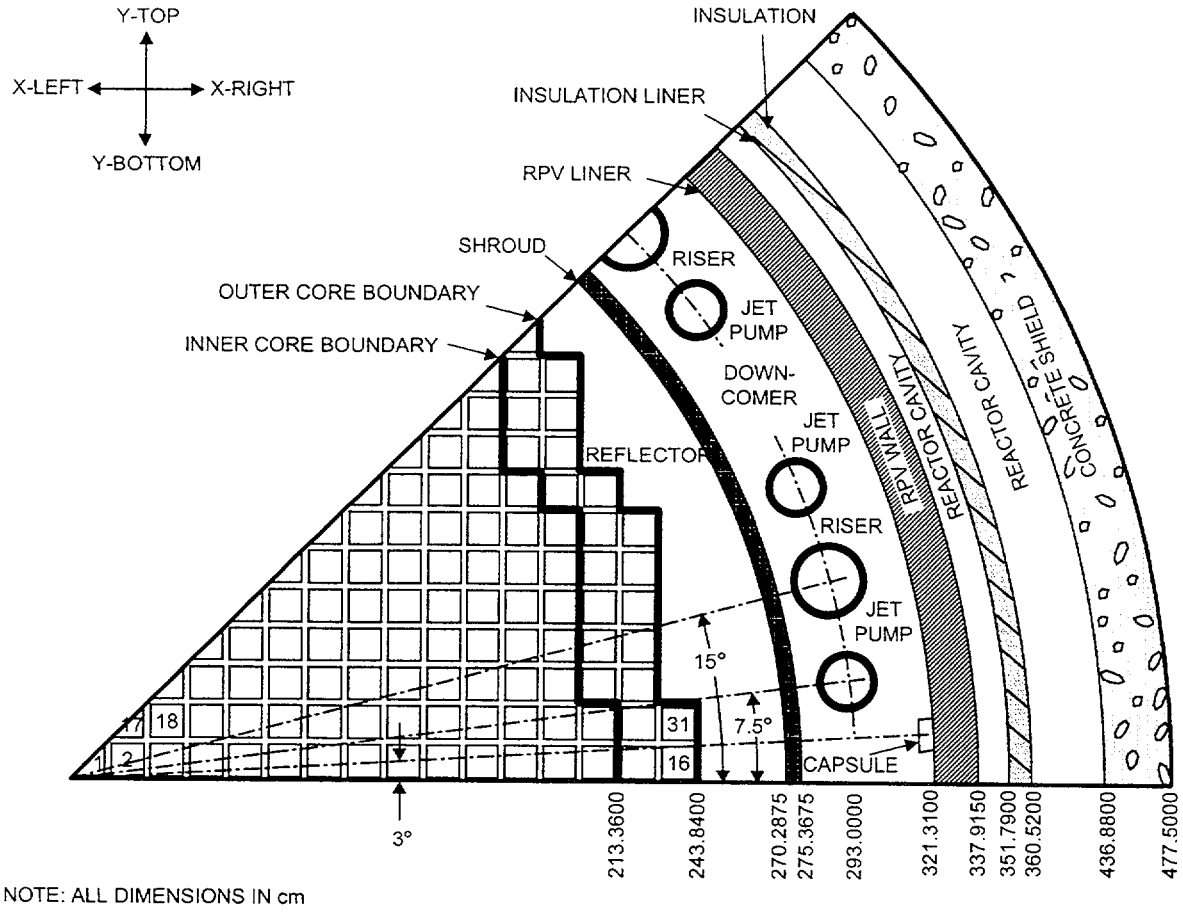

Figure 3-1. BWR Planar Geometry

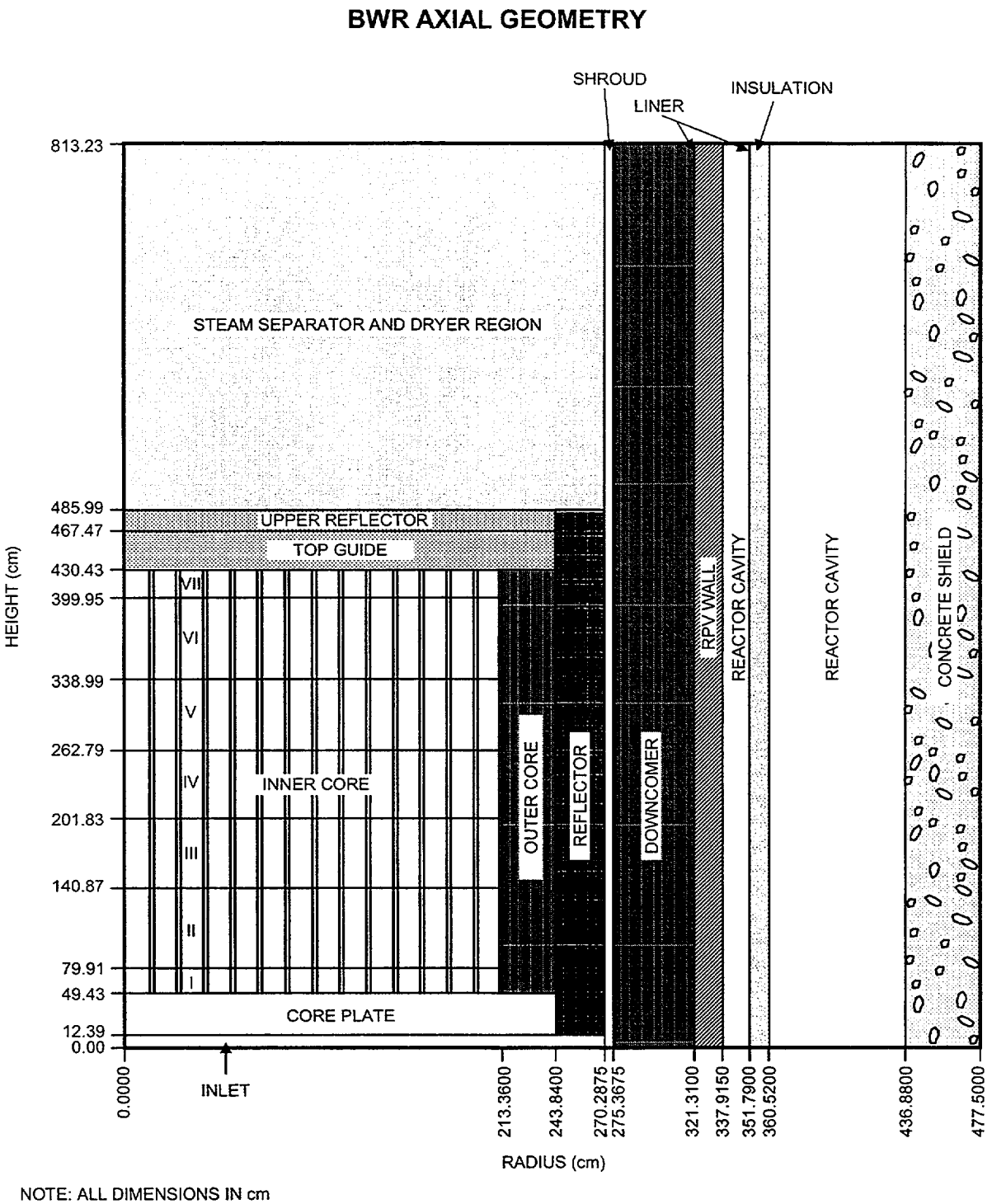

Figure 3-2. BWR Axial Geometry

Figure 3-3. Downcomer Flux (E>1 MeV) with Various Downcomer Models

Figure 3-4. RPV ID Flux (E>1 MeV) with Various Downcomer Models

Figure 3-5. RPV 1/4T Flux (E>1 MeV) with Various Downcomer Models

Figure 3-6. RPV T Flux (E>1 MeV) with Various Downcomer Models

Figure 3-7. Axial Flux Profile (E>1 MeV) at Various Radial Locations

Figure 3-8. GE vs. BNL Azimuthal Flux Profile (E>1 MeV) at Downcomer

Figure 3-9. GE vs. BNL Azimuthal Flux Profile (E>1 MeV) at RPV ID

Figure 3-10. GE vs. BNL Flux Spectra at RPV ID

Figure 3-11. GE vs. BNL Flux Spectra at RPV 1/2T

Figure 3-12. GE vs. BNL Flux Spectra at Capsule

Figure 3-13. GE vs. BNL Azimuthal Flux Profile (E>0.1 MeV) at Downcomer

Figure 3-14. GE vs. BNL Azimuthal Flux Profile (E>0.1 MeV) at RPV ID

Figure 3-15. ENDF/B-VI vs. ENDF/B-V Flux at RPV ID

Figure 3-16. ENDF/B-VI vs. ENDF/B-V Flux at RPV 1/4T

Figure 3-17. ENDF/B-VI vs. ENDF/B-V Flux at RPV OD

Figure 3-18. Pin-By-Pin vs. Bundle-Average Flux at Shroud ID

Figure 3-19. Pin-By-Pin vs. Bundle-Average Flux at RPV ID

Figure 3-20. S_{12} vs. S_8 Flux at Shroud ID

Figure 3-21. S_{12} vs. S_8 Flux at RPV ID

4.0 MONTE CARLO SOLUTION TO BWR BENCHMARK PROBLEM

4.1 INTRODUCTION

This section describes the GE Monte Carlo model of the benchmark problem developed for the NRC by BNL[2], using the code MCNP01A, a GE ECP version of MCNP[7]. The results obtained are compared with the BNL benchmark results. Two MCNP models are described: one where node average powers in the (r,θ) direction will be used to sample the source distribution, and the second where rod by rod power distributions will be used in varying degrees (2x2, 4x4, 8x8) for the three outermost sets of bundles. The calculations were performed using continuous energy ENDF/B-V data for all isotopes except oxygen (in water) and iron, where ENDF/B-VI data were used. Additionally, a third set of calculations was performed using ENDF/B-V data for all isotopes and a rod-by-rod description of the source term in the three outermost sets of bundles. A fourth set of calculations was performed for the rod-by-rod case to determine the sensitivity of the results to the actinide composition of the fuel.

4.2 ASSUMPTIONS

The model of the reactor and internals configurations is based on the description of the benchmark problem [2]. The actinide composition of the fuel is assumed to be uniform for all the fuel types and is taken to be that corresponding to a burnup of 14.12 GWd/t[2]. In the benchmark problem, the three burnup groups are given as 13.831, 13.788, and 12.755 GWd/t[2]. However, since the benchmark specifications did not provide data[2] at any of these specific values, a set closest to the 13.831 GWd/t value was taken to represent the actinide composition. A sensitivity case where the composition was changed to that corresponding to a burnup of 17.88 GWd/t was also made.

4.3 MODEL AND MATERIAL SPECIFICATIONS

The details of the geometric model can be found in Figures 3-1 and 3-2. The MCNP model does not include regions beyond the reactor cavity (just outside the RPV). From a standpoint of fuel composition, the model divided the core into an inner core and outer core in the (r,θ) plane, with the two outermost bundles assigned to the outer core, and all other bundles assigned to the inner core. Seven axial zones were modeled based on the description in Reference 2. An octant of the core and the ex-core regions was modeled with reflective boundary conditions.

The fuel material was modeled as homogenized fuel, clad, and in-channel water, and occupying a square inner box of dimension 12.924 cm on the side. The ex-channel water and channel zircalloy were homogenized into a second material that occupied everything outside of the fuel mixture in the node, which is the standard 15.24 cm on each side. The material compositions are

given in Table 3-5, with the exception of the jet pumps and risers. The jet pumps and risers in the three-dimensional calculations were modeled explicitly and therefore used the material compositions presented for jet pump and riser metal in Reference 2.

As described above, two basic models were developed, one with only one fuel region in all bundles and the other with 2x2, 4x4, and 8x8 regions in the second bundle from the periphery, the first bundle from the periphery, and the peripheral bundles, respectively. In all cases, the fuel composition remained the same; the reason for dividing the fuel region into finer regions was to apply the appropriate power levels at each axial node. The first of these models is referred to as the "smeared" case and the second would be referred to as the "rod" case during the rest of this Chapter. The repeated-structures capability in MCNP was used in the core region for both models.

The reflector region, shroud, downcomer, RPV liner, and RPV were modeled with sub-regions in order to facilitate importance sampling as a variance reduction technique. Beyond the RPV outer wall, the cavity region was also modeled. In the axial direction, the region below the core plate, core plate, top guide region, upper reflector region, and the steam separator regions were modeled. Figures 4-1, 4-2, and 4-3 show the MCNP representation of the smeared and rod (r,θ) views and the (r,z) view (generally representative of both models), respectively.

4.4 SOURCE SPECIFICATIONS

The neutron source was modeled using the generalized source card and volume sources. The cell feature was used for both the smeared and the rod cases. The probability distribution for the cells was obtained from the source distribution provided in Reference 2. The general (r,θ) source distribution for the smeared case is presented in Table 3-2. This source distribution is re-normalized such that $1/8^{th}$ of the total core power equals 1.0.

In the rod case, the x-y source distributions of the outer three layers of bundles were obtained from Reference 2. However, the rod-by-rod numbers presented in the benchmark report were multiplied by a peak axial factor (1.2575 for the full sub-nodes and 2.5150 for the half sub-nodes) for use in the 2-D calculations. In order for the rod-by-rod numbers to add up to the proper node average power, the rod-by-rod numbers were divided by the peak axial factors such that the total power is 1.0 for a $1/8^{th}$ core. There were some sub-nodes in bundles 103 and 106 that were outside the geometry of the system. Since this would present a problem for the source sampling, these nodes had their probabilities set to zero and the corresponding mirror reflected

sub-node (that was within the geometry) had its probability doubled. Thus, once again, the total power was preserved at 1.0.

The z source distribution (axial shape) was obtained from Table 2.2.2.6 of Reference 2. The distribution labeled 1 was used for the all the bundles except the last two layers. The distribution labeled 2 was used for the bundles next to the peripheral bundles. The distribution labeled 3 was used for the peripheral bundles.

The source energy distribution was based on a burnup of 14.12 GWd/t and was sampled from the thermal fission neutron distribution for U-235, U238, Pu-239 or Pu-241 with the probability of each isotope based on the distribution given in Table 2.2.1.1 of Reference 2. The fission spectrum and energy group structure for each of these isotopes were also obtained from Reference 2. As mentioned earlier, a sensitivity assessment to the burnup was performed and will be discussed later.

4.5 TALLY SPECIFICATIONS

All cases were run using a sample size of 320 million histories. All tally regions in the octant were divided into 20 azimuthal sectors each of 2.25°. The axial locations were chosen based on those chosen for the benchmark problem in Reference 2. Tallies were scored in the following regions, the axial extents of which were 4 cm:

- Downcomer in a region between 278.877 cm and 277.323 cm, with the center at 278.1 cm. Two cells with axial midpoints of 240 cm and 306 cm were tallied.
- RPV liner region with axial midpoints of 240 cm and 306 cm.
- RPV quarter thickness between 323.802 cm and 325.818 cm, with the center at 324.81 cm. Two axial cells with midpoints of 240 and 306 cm were tallied.
- RPV full thickness between 337.915 cm and 335.899 cm, with the center at 336.9 cm. Two cells with axial midpoints at 240 cm and 302 cm were tallied.
- Shroud tallies were between 271.304 cm and 270.288 cm with the center at 270.75 cm. Two cells with axial midpoints at 240 cm and 302 cm were tallied.
- A tally was made for a special run between the inner wall of the RPV at 321.786 cm and 324.5 cm in order to compare the MCNP results with the BNL MCNP results.

The tallies were made with volumes of 1 cm^3 for each region and the correct volume of each region was incorporated later. A problem cut-off of 0.1 MeV was used to speed up the calculation.

The fuel temperature used was chosen as 793K. The moderator and structural material, including the fuel cladding, were at the standard operating temperature of 559K. All runs were made using

Digital Alpha Stations which ran histories at the rate of approximately 75,000 – 87,000 histories per CPU minute.

4.6 ANALYSIS

4.6.1 MCNP Calculations and MCNP BNL Benchmark Calculations

The rod model was used as a base model and the results from these calculations were compared to the BNL benchmark MCNP results. MCNP results were presented in Reference 2 for two locations: the downcomer and quarter T (see Section 4.5 for definitions of tally regions). Figure 4-4 and Table 4-1 present the comparison of the two sets of data. A similar comparison can be made for the inner RPV location, and these are presented in Table 4-2 and Figure 4-5. All points in the figures are shown with 1σ error bars.

4.6.2 Sensitivity to the Cross Sections

The base rod case was run using ENDF/B-V data for all isotopes except oxygen and the iron isotopes for which ENDF/B-VI data was used. Two sensitivity runs were made to study the effects of the cross sections on the fluxes. The first used ENDF/B-V cross sections for all isotopes and the second used ENDF/B-VI cross sections for iron only. These results will be presented for the downcomer, liner, RPV- quarter T and full T locations. The error bars on the ENDF/B-VI for iron only are not shown for purposes of clarity in the figures. The ratios shown are taken with respect to the ENDF/B-V data, since the intent is to show the effect of moving to the ENDF/B-VI data for iron and oxygen from the existing ENDF/B-V data set.

The downcomer location data is presented in Figure 4-6. The results indicate that the effect of the cross sections at this location is very small and generally within one standard deviation of the ratios.

The next set of results in Figure 4-7 represent data at the RPV liner. These results also show an effect, which is within the uncertainty of the data. The quarter T position results are presented in Figure 4-8 and the full T position results are presented in Figure 4-9.

4.6.3 Sensitivity to Jet Pumps

The next series of sensitivities were performed to determine the effect of the jet pumps. The rod case was modified to replace the jet pumps and risers with water and tallies were made at the downcomer, RPV liner, RPV quarter T and the RPV full T and these were compared to the rod case.

The results at the downcomer are presented in Figure 4-10. As expected, the jet pumps have no effect at the downcomer locations. The liner results are presented in Figure 4-11. The effect of the jet pumps and risers are seen in the case of the liner. On the average, the fluxes in the case without the jet pump are about 15 percent higher than in the base case.

4.6.4 Sensitivity to Fission Source Distribution

The base case runs used a distribution of actinides based on a burnup of 14.12 GWd/t. Thus, based on the relative abundance of U-235, U-238, Pu-239, and Pu-241, the appropriate fission energy distribution was selected for each particle in the simulation. The purpose of this study was to determine the effect of changing the relative abundance of these four isotopes. A new run was made using the rod model and the distribution of these actinides based on 17.88 GWd/t[2]. The new source had a relative abundance of 51% U-235 (compared to 56% at the original burnup), 8% of U-238 (compared to 8% at the original burnup), 36% Pu-239 (compared to 32% at the original burnup), and 5% Pu-241 (compared to 4% at the original burnup).

4.6.5 Sensitivity to Bundle Source Distribution Model

The last set of sensitivity studies was performed to determine the effect of using rod-by-rod source distributions in the peripheral bundles compared to smeared sources. Figures 4-16 and 4-17 show the comparisons between the two cases for the downcomer and the RPV quarter T locations.

4.7 CONCLUSIONS

Table 4-1
Comparison of MCNP Calculations with Benchmark Data at 240 cm for Downcomer

Table 4-2
Comparison of MCNP Calculations with Benchmark Data at 240 cm for Inner RPV Location

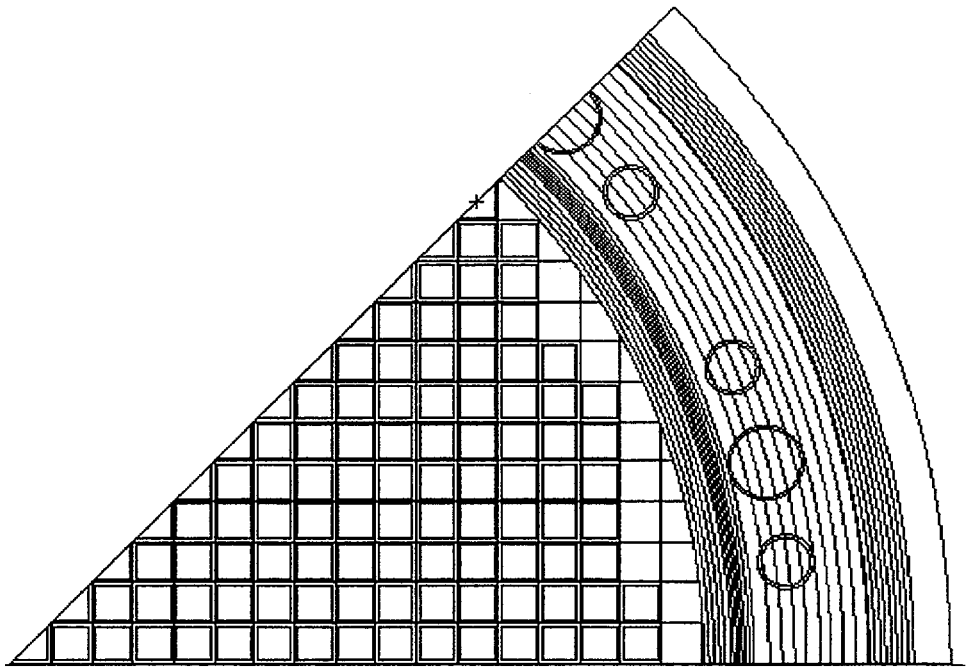

Figure 4-1. (R,θ) View of the Smeared Model

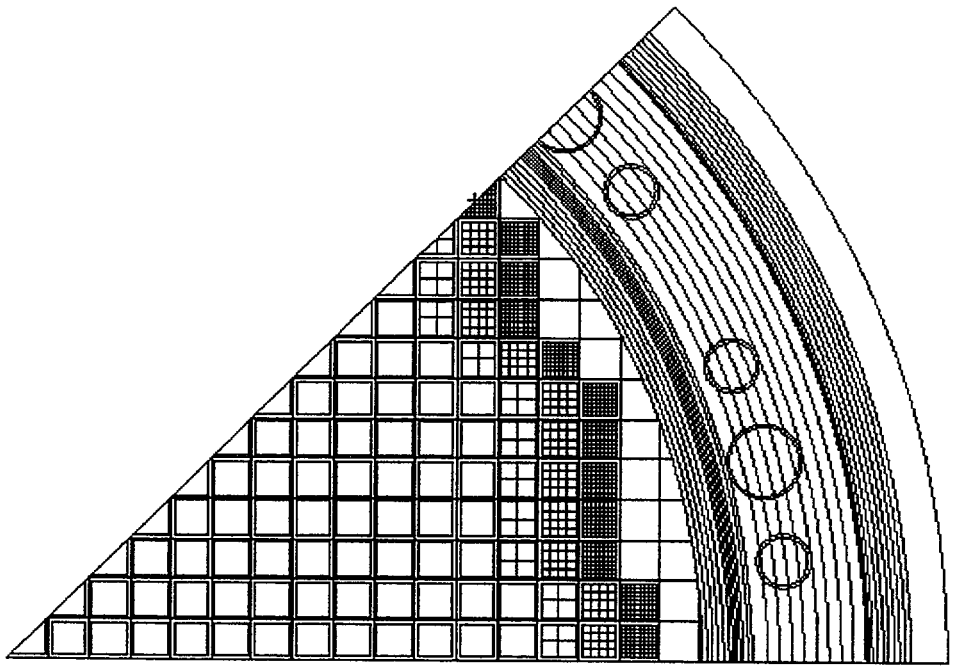

Figure 4-2. (R,θ) View of the Rod Model

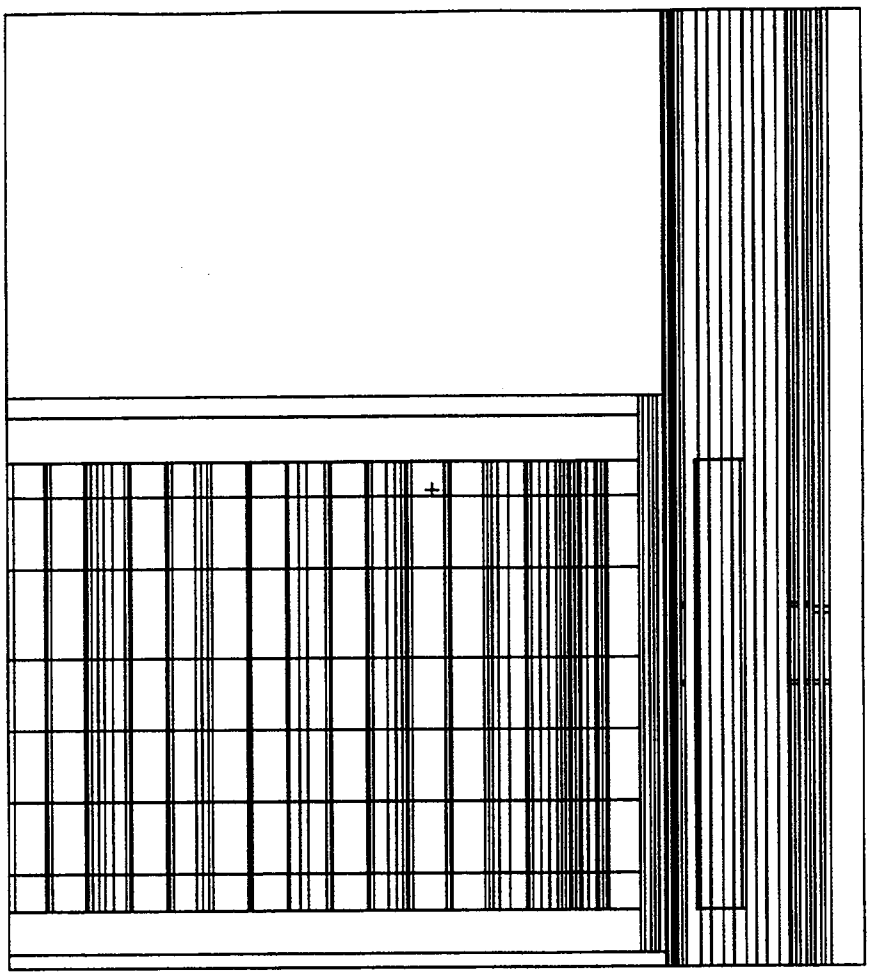

Figure 4-3. (R,Z) View of the Models

Figure 4-4. Comparison of MCNP and Benchmark MCNP Downcomer Fluxes at 240 cm

Figure 4-5. Comparison of MCNP and Benchmark MCNP Inner RPV Fluxes at 240 cm

Figure 4-6. Effect of Cross Section Sets on MCNP Flux at the Downcomer at 306 cm

Figure 4-7. Effect of Cross Section Sets on MCNP Flux at the RPV Liner at 306 cm

Figure 4-8. Effect of Cross Section Sets on MCNP Flux at the RPV Quarter T at 306 cm

Figure 4-9. Effect of Cross Section Sets on MCNP Flux at the RPV Full T at 302 cm

Figure 4-10. Effect of Jet Pumps on MCNP Fluxes at Downcomer at 306 cm

Figure 4-11. Effect of Jet Pumps on MCNP Fluxes at RPV Liner at 306 cm

Figure 4-12. Effect of Jet Pumps on MCNP Fluxes at RPV Quarter T at 306 cm

Figure 4-13. Effect of Jet Pumps on MCNP Fluxes at RPV Full T at 302 cm

Figure 4-14. Effect of Burnup on MCNP Fluxes at Downcomer at 306 cm

Figure 4-15. Effect of Burnup at RPV Quarter T at 306 cm

Figure 4-16. Effect of Bundle Source Distribution Model at Downcomer at 306 cm

Figure 4-17. Effect of Bundle Source Distribution Model at Quarter T at 306 cm

Figure 4-18. Effect of Bundle Source Distribution Model at Shroud at 306 cm

5.0 IN-REACTOR DOSIMETRY BENCHMARK

5.1 BACKGROUND

Regulatory Guide 1.190 calls for validation of the fluence calculation methodology by comparing the calculated results with both measurements and calculational benchmark. The fluence calculation methods must be validated against (1) operating reactor measurements that provide in-vessel surveillance capsules dosimetry or ex-vessel cavity measurements or both, (2) a pressure vessel simulator benchmark that provides measurements at the inner surface and at the T/4 and 3T/4 positions within the vessel, and (3) available fluence calculation benchmarks. The methods used to determine the plant-specific data and to calculate the benchmark solutions must be consistent to the extent possible with those used to calculate the vessel fluence. That is, the same cross sections, transport technique, and transport code parameters that are to be used in the reactor licensing application must be employed in the calculation of the benchmark measurements and reference calculations.

The calculation-to-measurement comparisons are used to identify biases in the calculations and to provide reliable estimates of the fluence uncertainties. When the measurement data are of sufficient quality and quantity that they allow a reliable estimate of the calculational biases (i.e., they represent a statistically significant measurement data base), the comparisons to measurement may be used to (1) determine the effect of the various modeling approximations and any calculational bias and, if appropriate, (2) modify the calculations by applying a correction to account for bias or by model adjustment or both.

In this section, calculations are compared to a set of in-reactor dosimetry measurements obtained from an operating BWR. These measurements serve the purpose of the simulator benchmark stipulated in RG 1.190.

5.2 DESCRIPTION OF MEASUREMENT BENCHMARK

A set of radiation and damage monitors was successfully installed in an overseas BWR4 plant during the summer of 1997, and removed following a cycle of operation during the summer of 1998[8,9]. The activated monitors were shipped to GE Vallecitos Nuclear Center (VNC) for processing. At VNC, the monitors were removed from their holders and sorted for counting and measurements to obtain the reaction rates of these monitors.

5.3 DORT CALCULATIONAL MODEL

The GE discrete ordinates flux solution methodology described in Section 2.1 is used to provide the 3-D flux distribution by constructing the synthesized results of (r,θ) and (r,z) calculations. All flux solution calculations are performed using an S_{12} quadrature and a P_3 Legendre polynomial expansions of the scattering cross sections.

5.3.1 Core Configuration

5.3.2 Cross Section Processing

5.3.3 Neutron Source Calculation

where,

1097 MWt is the rated thermal power

0.125 represents 1/8th of the core

381 cm is the total height of the core.

For the (r,z) calculation, the goal is to generate a relative, rather than absolute, flux magnitude. Therefore, a precise neutron source description is not essential. A typical number of 1.0E20 n/sec is used.

5.3.4 Modeling of Downcomer and Bypass Region

Since the focus of this benchmark is the dosimetry reaction rates in the downcomer at the 4°, 20°, and 71° azimuths, which are free of interference from the jet pumps and risers, these components are not modeled in this calculation.

5.3.5 Reaction Rate Calculation

The dosimeters in the capsules, after irradiation and post-processing of these dosimeters, result in measurement data in the unit of disintegration per second per gram of dosimeter isotope (dps/g). The corresponding calculated values can be derived and expressed in the following equation:

$$\frac{dps}{g} = \frac{N_A}{M} \sum_g \sigma_g \phi_g \sum_i p_i (1 - e^{-\lambda' \Delta t_i}) e^{-\lambda (t_{EOI} - t_i)}$$

where,

N_A = Avogadro's number (6.022×10^{23})

M = atomic mass of the dosimetry material

σ_g = dosimetry cross section for neutron energy group g

ϕ_g = neutron flux for group g

λ = decay constant for the daughter isotope of dosimeter isotope of interest

λ' = isotope removal constant, $\lambda + \sigma^r \phi$

σ^r = isotope removal cross section

t_i = time at the end of irradiation time step i

Δt_i = duration of irradiation time step i

t_{EOI} = time at the end of cycle irradiation

p_i = relative power for time step i.

5.3.6 Results

5.4 MCNP CALCULATIONS

5.4.1 Calculational Methodology

The In-Reactor Dosimetry experiment (see Section 5.2) was simulated using three-dimensional Monte Carlo methodology. The computational model was based on the code MCNP01A, a GE ECP version of MCNP[7], used in conjunction with ENDF/B-V and -VI cross section data. The model was developed in two stages.

In the first stage, a quadrant of the core was modeled with the full geometric and material details in the core. This included rod-by-rod description in each of 25 axial nodes (15.24 cm) for all 60 bundles in the quadrant. The important structural components inside the RPV were also included

and detailed water density distributions inside and outside the core were modeled. Four exposure points during the cycle were studied. At each point, a criticality run was performed and fast flux profiles, particularly in peripheral bundles, were compared with plant data. When these results compared within 10% at the periphery[10], the second stage of the calculations was performed using sources saved at the core periphery.

The fixed source calculations, one at each of the four exposure points, were used to obtain activation rates at the various wires. The fixed source model included details of the dosimetry packages present in the downcomer region, including clamp hardware used to keep the dosimeters in place during irradiation. Detailed water density distributions were used in the downcomer in the radial direction. A time integration with appropriate decay terms for each isotope under consideration was performed to properly add the results of the four separate runs to obtain the final specific activity of each wire at the End of Cycle (EOC) at every location. The test data specific activities were also presented at EOC. Figure 5-6 shows an (r,θ) view of the fixed source model (without the core) with dosimetry holders and other structural hardware.

5.4.2 Results

Results for three axial and radial locations for the three azimuths are shown in Tables 5-4a, 5-4b, 5-4c and 5-5a, 5-5b, 5-5c. The detector identification is as follows: "A", "B", and "C" represent the low, middle, and high axial locations. The first numeral "1", "2", and "3" represent the shroud, mid-annulus, and RPV locations. The second numeral represents the azimuth, 1 representing 20° (next to a jet pump), 2 representing 4° (away from jet pumps), and 3 representing 71° (between jet pumps) (see Figure 5-6). Tables 5-4a, 5-4b, and 5-4c show the fast response comparisons as C/M (calculation to measurement) ratios. The uncertainty associated with these fast responses is 13%.

The actinide responses agree well with test data at the shroud and tend to be under-predicted at the RPV. This is principally due to the fact that the neutron-to-gamma ratios fall rapidly when moving radially outward and the gamma induced fission becomes important. The calculations have ignored this contribution because the MCNP code does not have the capability of generating and tracking gamma induced neutrons. Thus the calculations under-predict the activities in a progressive manner as the capsule location changes from the shroud to the RPV. The remaining wires are consistent and are in good agreement with the test data. Tables 5-5a, 5-5b, and 5-5c present the thermal response comparisons, including those obtained from the helium measurements. The agreement between test data and calculational results is good everywhere, especially at the shroud location. The exceptions are at the high axial locations where the center location has a C/M ratio of 1.3 and the RPV location has a C/M ratio of 0.7. This trend was consistent for all the azimuths leading to the conclusion that the attachment hardware was not at the nominal position used in the model, thus perturbing the local thermal field.

5.5 CONCLUSIONS

Calculations of capsule reaction rates in the In-Reactor Irradiation Monitors (IRIM) indicate that good calculation-to-measurement comparisons for the reaction rates in the dosimetry capsules can be obtained using the current GE RPV flux evaluation methodology based on the DORT discrete ordinates transport code and the cross section processing process in the GE ECP library.

This is especially true for the capsules at 4° azimuth which is away from the jet pumps perturbation. For the ^{93}Nb dosimeters, the calculated reaction rates are within ~20% of the measurement for most capsule locations with the best estimate downcomer temperature distribution. With the base model, relatively high C/M ratios are found for the ^{54}Fe and ^{58}Ni dosimeters at the capsule locations near the vessel and the mid-annulus at the 20° azimuth. Applying a more realistic downcomer temperature distribution helps bring these C/M ratios closer to unity.

The MCNP results show C/M ratios to be for the most part within the 13% uncertainties associated with the results. The average C/M ratios for the fast wires are: 1.0 (± 0.07) at 4°, 1.02 (± 0.11) at both 20° and 71°. The average C/M ratios for the thermal wires, excluding the mid-annulus and RPV upper axial locations, are: 0.98 (± 0.09) at 4°, 1.02 (± 0.14) at 20° and 1.05 (± 0.13) at 71°.

Table 5-1
Dosimetry Capsule ID and Locations

Table 5-2
C/M Ratios of Reaction Rates for Non-Actinides with Base Model

Table 5-2
C/M Ratios of Reaction Rates for Non-Actinides with Base Model (Continued)

Table 5-3
C/M Ratios of Reaction Rates for Non-Actinides with Alternative Model

Table 5-3
C/M Ratios of Reaction Rates for Non-Actinides with Alternative Model (Continued)

Table 5-4a
Fast C/M Ratios at 4 Degrees

Det. ID	^{238}U			^{232}Th		^{237}Np			^{58}Ni	^{93}Nb shield	^{54}Fe	^{93}Nb bare	Mean*	σ*
	Cs	Zr	Ru	Cs	Zr	Cs	Zr	Ru						
A12	1.02	1.02	0.99	1.00	0.98	1.04	1.07	1.02	1.12	1.28	1.10	1.09	1.15	0.09
B12	0.95	0.94	0.98	0.99	0.93	0.96	1.01	1.01	0.96	1.13	0.95	1.03	1.04	0.10
C12	0.88	0.86	0.89	0.82	0.82	0.87	0.89	0.90	1.00	1.05	0.93	0.98	1.00	0.06
A22	0.77	0.74	0.75	0.79	0.71	0.86	0.86	0.84	0.96	1.05	1.07	1.06	1.03	0.05
B22	0.76	0.75	0.79	0.73	0.74	0.78	0.84	0.84	0.99	0.99	1.15	1.11	1.05	0.08
C22	0.74	0.71	0.76	0.70	0.72	0.75	0.78	0.80	0.98	0.95	0.99	0.95	0.96	0.03
A32	0.54	0.54	0.58	0.49	0.50	0.66	0.67	0.68	0.92	0.91	0.89	0.92	0.92	0.02
B32	0.56	0.55	0.60	0.50	0.51	0.65	0.70	0.74	0.97	0.95	0.88	0.89	0.93	0.04
C32	0.59	0.54	0.60	0.49	0.50	0.66	0.69	0.73	0.98	0.98	0.88	0.90	0.94	0.05

*Mean and σ for non-actinides only

Table 5-4b
Fast C/M Ratios at 20 Degrees

Det. ID	^{238}U			^{232}Th		^{237}Np			^{58}Ni	^{93}Nb shield	^{54}Fe	^{93}Nb bare	Mean*	σ*
	Cs	Zr	Ru	Cs	Zr	Cs	Zr	Ru						
A11	0.89	0.98	1.02	0.93	1.04	0.97	1.04	1.03	1.09	1.14	0.95	1.03	1.05	0.09
B11	0.91	0.97	1.02	0.97	1.08	0.97	1.03	1.05	1.15	1.18	1.21	1.22	1.19	0.04
C11	0.91	0.88	0.89	0.85	0.96	0.94	0.96	0.95	1.10	1.14	1.05	1.11	1.10	0.04
A21	0.75	0.73	0.74	0.76	0.74	0.85	0.84	0.82	0.90	1.03	0.98	1.00	0.98	0.14
B21	0.82	0.86	0.90	0.80	0.93	0.88	0.92	0.91	1.15	1.07	1.06	1.03	1.08	0.05
C21	0.82	0.78	0.80	0.83	0.84	0.85	0.85	0.84	1.02	1.09	1.07	1.05	1.06	0.10
A31	0.61	0.63	0.64	0.52	0.56	0.66	0.67	0.66	0.92	0.86	0.92	0.84	0.88	0.05
B31	0.56	0.57	0.63	0.48	0.57	0.68	0.71	0.72	0.90	0.89	0.93	0.90	0.91	0.09
C31	0.57	0.55	0.60	0.53	0.60	0.63	0.66	0.68	0.92	0.88	0.90	0.86	0.89	0.03

* Mean and σ for non-actinides only

Table 5-4c
Fast C/M Ratios at 71 Degrees

Det. ID	^{238}U			^{232}Th		^{237}Np			^{58}Ni	^{93}Nb shield	^{54}Fe	^{93}Nb bare	Mean *	σ*
	Cs	Zr	Ru	Cs	Zr	Cs	Zr	Ru						
A13	0.82	0.80	0.79	0.81	1.11	0.89	0.98	0.85	0.79	1.05	0.90	1.03	0.94	0.12
B13	0.94	0.98	1.01	0.95	1.11	0.95	1.04	1.02	1.04	1.18	1.14	1.21	1.14	0.07
C13	0.90	0.93	0.96	0.88	0.89	1.01	1.01	1.03	1.07	1.16	1.18	1.23	1.16	0.06
A23	0.82	0.85	0.86	0.83	1.11	0.88	1.03	0.91	1.10	1.09	1.03	1.01	1.06	0.05
B23	0.83	0.81	0.82	0.85	0.97	0.88	0.91	0.87	0.99	1.07	1.04	1.05	1.04	0.04
C23	0.88	0.88	0.92	0.86	0.84	0.88	0.86	0.91	1.14	1.15	1.12	1.08	1.12	0.03
A33	0.59	0.60	0.61	0.57	0.77	0.61	0.72	0.64	0.84	0.83	0.87	0.81	0.84	0.03
B33	0.63	0.64	0.68	0.57	0.69	0.70	0.72	0.71	0.98	0.96	0.89	0.91	0.93	0.04
C33	0.58	0.56	0.62	0.56	0.56	0.71	0.66	0.72	0.93	0.94	0.93	0.90	0.93	0.02

* Mean and σ for non-actinides only

Table 5-5a
Thermal C/M Ratios at 4 Degrees

Det. ID	^{235}U			^{45}Sc	He	Mean	σ
	Cs	Zr	Ru				
A12	1.11	1.12	1.10	1.11	0.96	1.08	0.07
B12	1.02	1.02	1.18	0.98	1.01	1.04	0.08
C12	1.10	1.10	1.29	0.90		1.10	0.16
A22	0.92	0.94	0.99	0.82	0.85	0.91	0.07
B22	1.00	1.05	1.16	0.81	0.94	0.99	0.13
C22	1.38	1.38	1.59	1.12		1.37	0.20
A32	0.89	0.91	0.97	0.81		0.89	0.07
B32	0.87	0.88	1.00	0.73		0.87	0.11
C32	0.79	0.79	0.94	0.63		0.79	0.12

Table 5-5b
Thermal C/M Ratios at 20 Degrees

Det. ID	^{235}U			^{45}Sc	^{59}Co	He	Mean*	σ*
	Cs	Zr	Ru					
A11	1.02	1.02	0.98	0.97	1.20		1.05	0.09
B11	1.00	1.06	1.20	0.83	1.09		1.04	0.13
C11	0.93	0.96	1.13	0.81	0.99	No He	0.96	0.11
A21	0.81	0.82	0.87	0.73	0.78		0.80	0.05
B21	1.04	1.15	1.33	0.89	1.28		1.14	0.18
C21	1.39	1.38	1.54	1.12	1.38		1.36	0.15
A31	1.21	1.27	1.36	1.04	1.28		1.23	0.12
B31	0.91	0.92	1.06	0.75	1.03		0.94	0.12
C31	0.70	0.70	0.83	0.55	0.68		0.69	0.10

Table 5-5c
Thermal C/M Ratios at 71 Degrees

Det. ID	^{235}U			^{45}Sc	^{59}Co	He	Mean*	σ*
	Cs	Zr	Ru					
A13	0.98	1.00	1.00	1.01	1.30		1.06	0.13
B13	0.99	1.08	1.10	1.01	1.15	1.08	1.07	0.06
C13	1.00	1.03	1.04	0.84	1.14	0.92	1.00	0.10
A23	0.86	0.89	0.88	0.78	0.87		0.86	0.04
B23	1.19	1.29	1.29	0.97	1.15	1.25	1.19	0.12
C23	1.33	1.36	1.36	1.08	1.37	1.38	1.31	0.12
A33	1.23	1.26	1.26	1.06	1.39		1.24	0.12
B33	0.96	0.99	0.99	0.84	1.05		0.96	0.08
C33	0.74	0.72	0.72	0.57	0.84		0.72	0.10

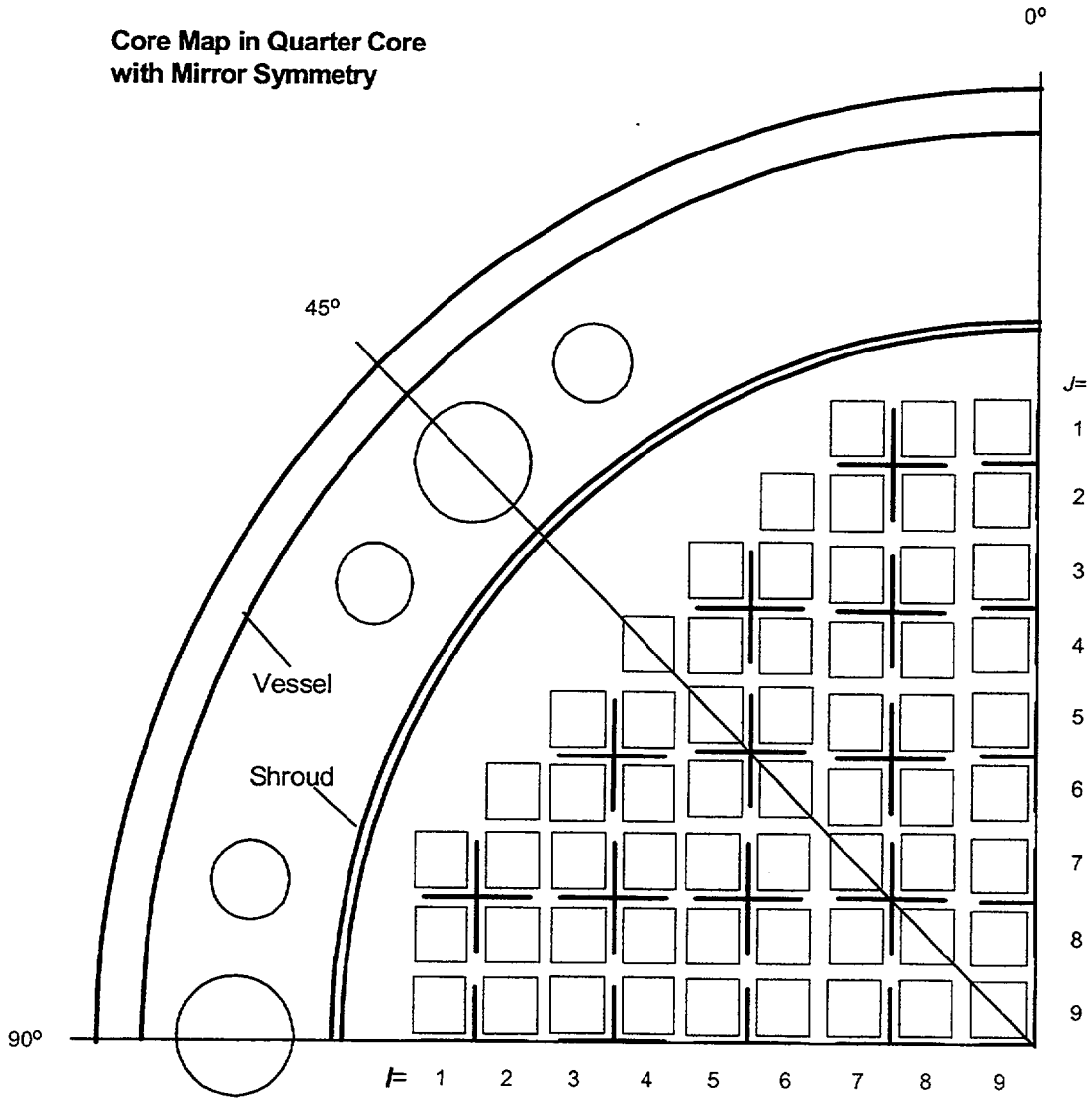

Figure 5-1. Schematic of a Quadrant of the Reactor Core

Figure 5-2. Relative Power Density at Core Midplane

Figure 5-3. Axial Nodal Power of Peripheral Bundles

Figure 5-4. C/M Ratios of Reaction Rates with Base Model

Figure 5-5. C/M Ratios of Reaction Rates with Alternative Model

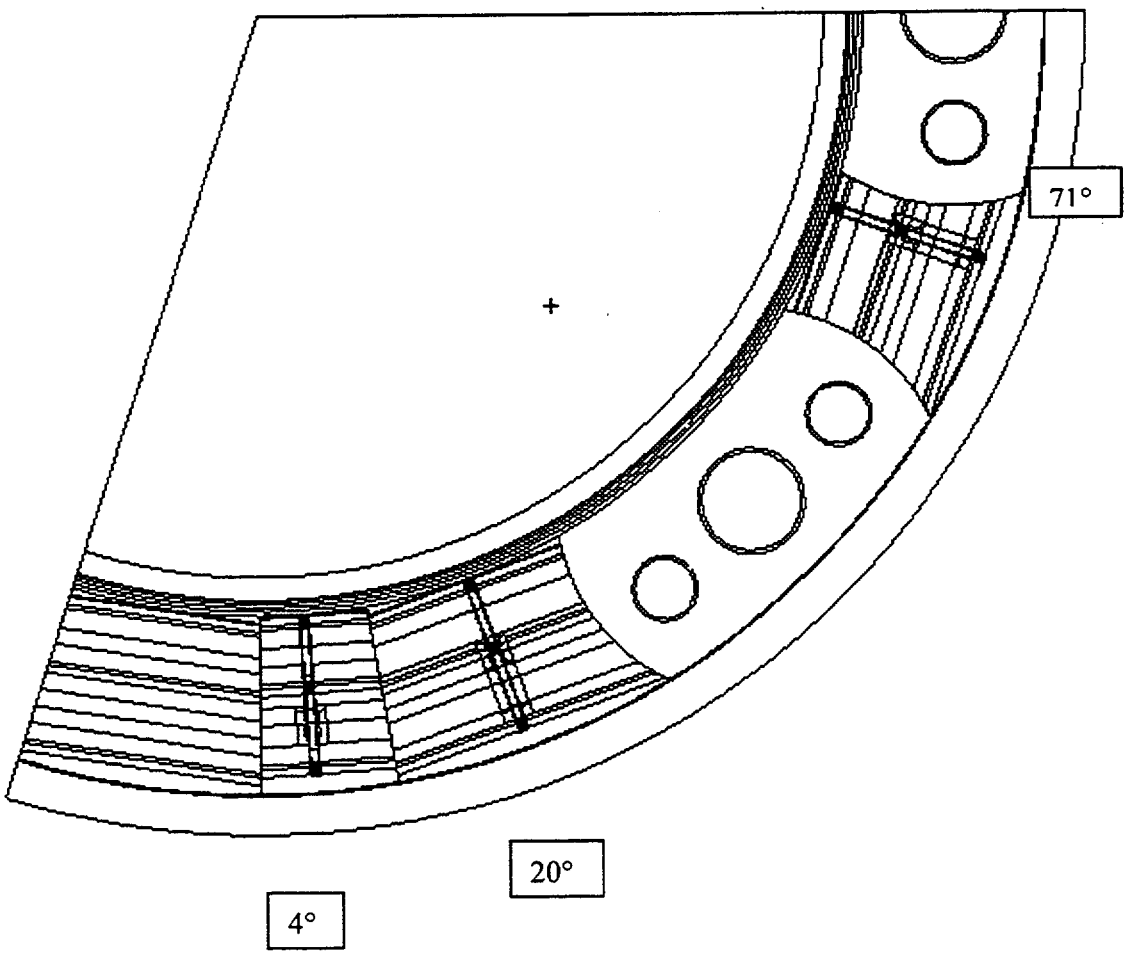

Figure 5-6. (R,θ) View of the MCNP Model with Capsule Holders

6.0 BWR SURVEILLANCE SAMPLE DATA

6.1 SURVEILLANCE DATA

A representative list of flux data generated by GE during the past decade is shown in Table 6-1.

The calculated flux values at surveillance capsule locations were the result of GE traditional discrete ordinates calculations, using the coolant-only downcomer model and bundle-average power density, in conjunction with ENDF/B-V cross section library.

The dosimetry data obtained through surveillance samples were analyzed by the Vallecitos Nuclear Chemistry Facility (VNC). The majority of surveillance capsules contain iron, copper, and nickel wires. Since Co-58 has a relatively short half-life compared to activation products of iron and copper, the nickel wire reading could differ significantly from those of iron and copper. Therefore in some of the dosimetry reports, the result of nickel wires was discounted. In other older reports, data for individual flux wires were not given, instead a single flux value was reported. The methodology and process for the VNC dosimetry analysis are detailed in Section 6.2.

6.2 MEASURED FLUX UNFOLDING FROM SURVEILLANCE DATA

6.2.1 Basic Equations

The power history for use in dosimetry analysis is obtained from plant operating data applicable to period of residence of the dosimetry capsule in the reactor. The power history or the total amount of energy generated can be obtained on a variety of bases ranging from a daily breakdown to larger time periods. Based on this information, the effective full power fraction can be derived. The effective full power fraction, p_i, is defined as P_i/P, where P is the full power of the core and P_i is the power during the time interval $(t_i - t_{i-1})$. Therefore, if ϕ_P is the full power flux, the actual flux during this time interval is

$$\phi_i = p_i \phi_P \tag{1}$$

The total specific activity of a dosimeter wire in disintegrations per second per gram of target isotope (dps/g) at the end of irradiation (EOI) may be expressed as

$$\frac{dps}{g} at\ EOI = \frac{N}{\rho}\sigma\phi_P \sum_i p_i (1 - e^{-\lambda(t_i - t_{i-1})}) e^{-\lambda(t_{EOI} - t_i)} \tag{2}$$

where

N = atomic density of the target isotope (atoms/cm^3)
σ = microscopic activation cross section for target isotope (cm^2)
ρ = mass density of target isotope (g/cm^3)

t_{EOI}= time at end of irradiation (s)
λ = decay constant of daughter isotope (s^{-1})

The first term with the exponential in Equation 2 accounts for the build-up and decay of the daughter isotope at the flux level ϕ_i, while the second term accounts for the decay during the remainder of the time to EOI. It must also be noted that the decay constant used in the first term with the exponential is strictly defined as $\lambda' = \lambda + \sigma\phi$, where $\sigma\phi$ represents the removal of the daughter isotope by neutron absorption. However, typically this term is negligible when compared to the radioactive decay constant. Therefore, the expression in Equation 2 contains only the decay constant, λ. The sum over each time step represents the actual measured specific activity at EOI. Inverting Equation 2,

$$\phi_P = \frac{\frac{dps}{g}}{\frac{N}{\rho}\sigma\sum_i p_i(1-e^{-\lambda(t_i-t_{i-1})})e^{-\lambda(t_{EOI}-t_i)}} \tag{3}$$

Substituting for N,

$$N = \frac{\rho N_A}{M} \tag{4}$$

where,

N_A = Avogadro's number (atoms/mole)
M = mass of one mole of the target isotope (g/mole).

The full power flux

$$\phi_P = \frac{\frac{dps}{g}\cdot M}{N_A\sigma\sum_i p_i(1-e^{-\lambda(t_i-t_{i-1})})e^{-\lambda(t_{EOI}-t_i)}} \tag{5}$$

The accumulated fluence over the period ending at EOI is then given by

$$Fluence = \phi_P\sum_i p_i(t_i - t_{i-1}) \tag{6}$$

The term under the summation sign is the effective time the reactor was operating at full power.

6.2.2 Cross Section Evaluation

In the expressions presented in Section 6.1.1, the effective activation cross section, σ, needs to be defined. Typically, in BWR surveillance programs there are only two wires, Fe and Cu. The cross sections used for this purpose are derived from two correlations developed by GE for the Fe-54 and Cu-63 activation reactions.

A multiple dosimeter, full spectrum unfolding code[11] which determined a neutron spectrum and integral fluxes using activation data from irradiated dosimeters was obtained for application to GE Nuclear experiments.

A qualification program for the generation of neutron spectra from activation detectors was undertaken by the IAEA where two reaction rate sets were sent to international participants for intercomparison. These sets were the only information about the spectra which could be used by the participants, who, in turn, had to use their own program, cross sections, etc., to generate neutron spectra. GE participated in this program with results which ranked fourth (among 59) and first (among 34) for the two cases evaluated[12]. Thus, the spectral unfolding code was independently benchmarked and qualified for use in spectral unfolding experiments at GE.

The code was later modified such that trial input spectra were automatically selected from a library containing several neutron spectra. The differential cross section library input originally was ENDF/B-IV and later updated to ENDF/B-V.

Over the years the GE code was successfully used for several spectral determinations at BWR and General Electric Test Reactor locations, as well as at the Advanced Test Reactor (ATR) at Idaho Falls.

6.2.3 Uncertainty in the Cross Sections

6.2.4 ASTM Standards

All the measurement methodologies applied were compliant with the following ASTM standards:

1. ASTM Designation E181-93, *Standard Test Methods for Detector Calibration and Analysis of Radionuclides*, ASTM Standards, Section 12, American Society for Testing and Materials, Philadelphia, PA, 1995.
2. ASTM Designation E261-90, *Standard Practice for Determining Neutron Fluence Rate, Fluence, and Spectra by Radioactivation Techniques*, ASTM Standards, Section 12, American Society for Testing and Materials, Philadelphia, PA, 1995.
3. ASTM Designation E263-93, *Standard Method for Measuring Fast-Neutron Reaction Rates by Radioactivation of Iron*, ASTM Standards, Section 12, American Society for Testing and Materials, Philadelphia, PA, 1995.
4. ASTM Designation E264-92, *Standard Method for Measuring Fast-Neutron Reaction Rates by Radioactivation of Nickel*, ASTM Standards, Section 12, American Society for Testing and Materials, Philadelphia, PA, 1995.
5. ASTM Designation E523-92, *Standard Test Method for Measuring Fast-Neutron Reaction Rates by Radioactivation of Copper*, ASTM Standards, Section 12, American Society for Testing and Materials, Philadelphia, PA, 1995.
6. ASTM Designation E844-86 (Reapproved 1991), *Standard Guide for Sensor Set Design and Irradiation for Reactor Surveillance*, ASTM Standards, Section 12, American Society for Testing and Materials, Philadelphia, PA, 1995.
7. ASTM Designation E1005-84, *Standard Test Method for Application and Analysis of Radiometric Monitors for Reactor Vessel Surveillance*, ASTM Standards, Section 12, American Society for Testing and Materials, Philadelphia, PA, 1995.

8. ASTM Designation E1297-89, *Test Method for Measuring Fast Neutron Reaction Rates by Radioactivation of Nb,* ASTM Standards, Section 12, American Society for Testing and Materials, Philadelphia, PA, 1995.

9. ASTM Designation E704-90, *Test Method for Measuring Reaction Rates by Radioactivation of U-238,* ASTM Standards, Section 12, American Society for Testing and Materials, Philadelphia, PA, 1995.

10. ASTM Designation E705-90, *Test Method for Measuring Reaction Rates by Radioactivation of Np-237,* ASTM Standards, Section 12, American Society for Testing and Materials, Philadelphia, PA, 1995.

Table 6-1
Collective RPV Flux Data

Table 6-2
Fast Cross Sections (>1 MeV) for Iron and Copper Activation in BWRs

Table 6-3a
Fast (>1 MeV) Cross Sections in barns for a Dosimetry Capsule Location at a Distance 32.55 inches from the Core Edge

Table 6-3b
Fast (>1 MeV) Cross Sections in barns for a Dosimetry Capsule Location at a Distance 28.33 inches from the Core Edge

Table 6-3c
Fast (>1 MeV) Cross Sections in barns for a Dosimetry Capsule Location at a Distance 29.41 inches from the Core Edge

Table 6-3d
Fast (>1 MeV) Cross Sections in barns for a Dosimetry Capsule Location at a Distance 25.27 inches from the Core Edge

Table 6-3e
Fast (>1 MeV) Cross Sections in barns for a Dosimetry Capsule Location at a Distance 25.58 inches from the Core Edge

7.0 UNCERTAINTY AND BIAS ASSESSMENTS

7.1 CALCULATION UNCERTAINTIES

7.2 CALCULATION BIASES

7.2.1 Analytical Bias Assessment

7.2.2 Bias Derived from Historical Data

7.2.3 Applicability of Calculation Bias

7.3 OVERALL CALCULATION UNCERTAINTY

7.4 BEST-ESTIMATE FLUX AT REACTOR VESSEL

7.5 SHROUD FLUX UNCERTAINTIES AND BIASES

Table 7-1
RPV Flux Data for Bias Determination

8.0 CONCLUSIONS

9.0 REFERENCES

1. Regulatory Guide 1.190, "Calculational and Dosimetry Methods for Determining Pressure Vessel Neutron Fluence," USNRC, March 2001.
2. NUREG/CR-6115, "PWR and BWR Pressure Vessel Fluence Calculation Benchmark Problems and Solutions," USNRC, May 1997.
3. CCC-543, "TORT-DORT Two- and Three-Dimensional Discrete Ordinates Transport Version 2.8.14," Radiation Shielding Information Center, Oak Ridge National Laboratory.
4. Letter, S.A. Richards (USNRC) to G. A. Watford, "Amendment 26 to GE Licensing Topical Report NEDE-24011-P-A, GESTAR II – Implementing Improved GE Steady-State Methods (TAC No. MA6481)," November 10, 1999.
5. R. E. MacFarlane and D. W. Muir, "The NJOY Nuclear Data Processing System, Version 91," LA-12740-M, Los Almos National Laboratory, October 1994.
6. Nuclides & Isotopes, Fifteenth Edition, GE Nuclear Energy 1996.
7. Briesmeister, J., Ed., "MCNP - A Monte Carlo N-Particle Transport Code, Version 4A," LA12625, March 1994.
8. Terhune, J.H., Sitaraman, S., Higgins, J. P., Chiang, R-T, and Asano, K., "Neutron and Gamma Spectra in the BWR- Phase 1 Experimental and Computational Methods," Proceedings of the 5th International Conference on Nuclear Engineering, Nice, France, ICONE5-2020, May 26-30, 1997.
9. Sitaraman, S., Chiang, R-T., Asano, K., and Koyabu, K., "Benchmark for a 3D Monte Carlo Boiling Water Reactor Fluence Computational Package - MF3D", International Conference on Advanced Monte Carlo for Radiation Physics, Particle Transport Simulation and Applications, Lisbon, Portugal, October 23-26,2000.
10. Chiang, R-T. and Sitaraman, S., "Development of 3D MCNP-Based BWR Fluence Computational Software Package: MF3D," *Reactor Dosimetry, ASTM STP 1398,* John G. Williams, David W. Vehar, Frank H. Ruddy and David M. Gilliam, Eds., American Society for Testing and Materials, West Conshohocken, PA, 2000.
11. G. DiCola and A. Rota, "RDMM- A Code for Fast Neutron Spectra Determination by Activation Analysis", EUR-2985e, 1966.
12. "International Intercomparison of Neutron Spectra Evaluating Methods Using Activation Detectors", prepared by A. Fischer, Berichte der Kernforschungsanlage Julich-Nr. 1196, June 1975.